Czech Technical University in Prague

Faculty of Electrical Engineering

MASTER THESIS

Denis Efremov

Unstable ground vehicles and artificial stability systems

Department of Control Engineering

Supervisor of the master thesis: Doc. Ing. Martin Hromčík, Ph.D.

Study programme: Cybernetics and Robotics

Specialization: Systems and Control

Prague 2018

ZADÁNÍ DIPLOMOVÉ PRÁCE

I. OSOBNÍ A STUDIJNÍ ÚDAJE

Příjmení: **Efremov** Jméno: **Denis** Osobní číslo: **420311**

Fakulta/ústav: **Fakulta elektrotechnická**

Zadávající katedra/ústav: **Katedra řídicí techniky**

Studijní program: **Kybernetika a robotika**

Studijní obor: **Systémy a řízení**

II. ÚDAJE K DIPLOMOVÉ PRÁCI

Název diplomové práce:

Nestabilní pozemní vozidla a systémy pro jejich aktivní stabilizaci

Název diplomové práce anglicky:

Unstable ground vehicles and artificial stability systems

Pokyny pro vypracování:

The goal of the thesis is to investigate the flight-controls results of the 1980's related to statically unstable aircraft equipped with artificial stabilization systems (CCV, control-configured vehicles), and investigate their applicability for design of highly-manevourable high-performance cars.
1. Adopt suitable high-fidelity and low-fidelity lateral-dynamics simulation models.
2. Prepare variants with high, reduced, neutral, and lost stability.
3. Realize simulated ride tests on the simulation platform.
4. Investigate and design suitable control laws for lateral dynamics artificial stabilization, and realize related simulated ride tests.
5. Investigate estimation algorithms that can be useful to compensate for missing essential measurements, namely the tyre-models-based observers for estimation of the sideslip angle.

Seznam doporučené literatury:

[1] Edward M. Kasprzak, L. Daniel Metz, William F. Milliken Douglas L. Milliken, Race Car Vehicle Dynamics - Problems, Answers and Experiments, Premiere Series Books, 2015, ISBN-10: 0768011272.
[2] Sigur Skogestad, Ian Postletwaite, Multivariable feedback control, Wiley, 2015, ISBN-10: 0470011688.

Jméno a pracoviště vedoucí(ho) diplomové práce:

doc. Ing. Martin Hromčík, Ph.D., katedra řídicí techniky FEL

Jméno a pracoviště druhé(ho) vedoucí(ho) nebo konzultanta(ky) diplomové práce:

Datum zadání diplomové práce: **15.02.2018** Termín odevzdání diplomové práce: **25.05.2018**

Platnost zadání diplomové práce: **30.09.2019**

doc. Ing. Martin Hromčík, Ph.D.	prof. Ing. Michael Šebek, DrSc.	prof. Ing. Pavel Ripka, CSc.
podpis vedoucí(ho) práce	podpis vedoucí(ho) ústavu/katedry	podpis děkana(ky)

Acknowledgements

I would like to thank my supervisor doc. Ing. Martin Hromčík, Ph.D. for his valuable advice, ideas, and support during the creation of this master thesis.

Great thanks also belong to my colleges: Bc. Vít Cibulka for excellent help with the simulator; Bc. Marek László for his critics, which helped during this work. Also, I would like to thank my opponent, Ing. Martin Mondek, without his advice and his master thesis this work would never exist.

Mainly I would like to thank my family for invaluable help with my education, and my girlfriend and friends, without whom this thesis would not be completed.

I hereby declare that I have completed this thesis with the topic "Unstable ground vehicles and artificial stability systems" independently and that I have included a full list of used references. I have no objection to the usage of this work in compliance with the act §60 Zákon č.121/2000 Sb. (copyright law).

In ..... date ..... signature of the author

Abstrakt:

Cílem této diplomové práce je definovat pozemní vozidlo s nestabilní boční dynamikou pomocí názvosloví zavedeného Společností automobilových inženýrů, porovnat klady a zápory nestabilních aut, prodiskutovat možnosti jejich stabilizace pomocí systému aktivního řízení založeného na sledování reference na rychlost změny směru. Na konci této práce jsou porovnávány různé řídicí přístupy, jsou diskutovány algoritmy pro odhad skluzu a silová zpětná vazba na volant.

Klíčová slova: Nestabilní Pozemní Vozidlo; Umělé Stabilizační Systémy; Sledování Rychlosti Změny Směru; Přetáčivá Auta; Silová Zpětná Vazba; Odhad Bočního Skluzu; Odhad Skluzu Pneumatiky; Jednostopý Model; Pacejka Magic Formula; Steer-by-Wire.

Abstract:

This master thesis aims to define laterally unstable ground vehicle regarding the nomenclature introduced by Society of Automotive Engineers, lists pros & cons of making cars to be unstable, to discuss the possibilities of their stabilization by active steering system based on yaw rate tracking control architectures. At the end of this work, different control approaches are compared, slip estimation algorithms and force feedback are discussed.

Keywords: Laterally Unstable Ground Vehicle; Artificial Stabilization Systems; Yaw Rate Tracking; Oversteering Cars; Force Feedback; Side-Slip Estimation; Tire's Slip Estimation; Singel-Track Model; Pacejka Magic Formula; Steer-by-Wire.

Contents

1. Introduction

According to the Oxford dictionary, science is "the intellectual and practical activity encompassing the systematic study of the structure and behavior of the physical and natural world through observation and experiment." A scientist is always a romantic man, who answers the most interesting question in the world: "What if?"

After the design of the first successful airplane made by the Wright brothers, many scientists and engineers were charged to invent faster and agiler aircraft driven by the question: "What if?"

During the first half of the 20th century, the physics behind the airplanes have been described. The equations of flight have been derived. Researchers arrived to an understanding of the weight of each parameter in these equations. They were trying to answer the question: "What if?"

These attempts have borne their fruits. In 1980's the first statically unstable aircraft equipped with artificial stabilization systems took off in the sky. It was the control-configured version of Jaguar fighter, in witch regulators were used to stabilize the aircraft at supersonic speeds, where it is unstable [16]. The epoch of the new generation of agiler fighters began. Because of the most interesting question for every scientist: "What if?"

This thesis is inspired by results of that works behind the unstable aircraft and trying to answer the question: "What if?" Namely, "What if we create a laterally unstable ground vehicle?"

1.1 Outline

This work is divided into ten parts.

In the first two parts, which are [**Introduction**] and [**Objectives**], work description and goals are stated.

The part [**Used Vehicle Modelling Approaches**] introduces used vehicle's and tire's modelling techniques.

In part, which is named [**Laterally Unstable Vehicle**], the laterally unstable vehicle defined and its pros and cons are listed.

The 5th chapter, which is [**Proposed Control Architectures**], describes the possible control architectures which can be used to stabilize the laterally unstable ground

vehicle.

Chapter [**Simulation Tests**] shows the simulation results and comparison of the proposed control architectures.

The next two chapters are presented here just for completeness of the work because it was not a primary purpose of the thesis. The sixth part, which is named [**Slip Estimation Algoritms**], provides a short overview of the slip angle estimation algorithms.

In part [**Force Feedback**], the steer-by-wire vehicle is overviewed. Also, a force feedback design implemented in the simulator is shown.

The next part, [**Results**], lists reached goals.

The last part, [**Conclusion**] summarises this thesis and proposes possible future works in the field of laterally unstable ground vehicles.

2. Objectives

The primary objectives of this thesis are:

- Adopt suitable lateral-dynamics simulation model
- Define lateral instability of a ground vehicle
- Create a simulator based platform
- Investigate possible control techniques for a laterally unstable ground vehicle
- Realize simulated ride tests
- Investigate estimation algorithms that can be useful to compensate for missing essential measurements

3. Used Vehicle Modelling Approaches

3.1 Introduction

This chapter describes used vehicle modeling approaches and tire models. The proposed models were used to analyze a lateral vehicle dynamics and to compare different control techniques.

The nonlinear single-track model is derived in the section [**Nonlinear Single-Track Model**], its liniarization is provided in the next section [**Linearized Single-Track Model**], the last section [**Tyre Modelling Approaches**] describes the used tire modeling techniques.

3.2 Nonlinear Single-Track Model

For vehicle models there exist two main modeling techniques, which are mainly used to describe the vehicle dynamics: single-track [1, chapter 9] and twin-track models [1, chapter 10]. During this work, the first one was used, because it has sufficient fidelity for describing a lateral vehicle dynamics, used in a huge amount of articles touching lateral vehicle dynamics [2,3,4,5] and it is simpler than the second one (three versus sixteen states).

The same modeling technique was used in work of my predecessor, M. Mondek in [6]. But his model derivation begins with a creation of an equilibrium of all forces acting on a vehicle's center of gravity along x and y axis and moments acting around the z axis. In this work, the derivation begins with the derivation of equations of lateral, longitudinal and yaw motion. Also, here all nonlinearities are abandoned in the state space representation (Eq. 3.6). Despite differences in nonlinear models, resulting linearized models are the same.

3.2.1 Used assumptions and simplifications

The nonlinear single-track model is used to describe planar vehicle motion. The derivation of the model is used in the following articles: [2,3]. Used simplifications during the derivation have been [1]:

- All lifting, rolling, and pitching motion is neglected.
- Vehicle mass is assumed to be concentrated at the center of gravity.

- Front and rear tires are represented as one single tire on each axle. Imaginary contact points of tires and surface are assumed to lie along the center of axles.
- Pneumatic trail and aligning torque resulting from a side-slip angle of a tire are neglected.
- Mass distribution on the axles is assumed to be constant.
- Longitudinal forces on tires, resulting from a normalized tire slip angle, are neglected. All longitudinal forces acting on each axle are assumed to be strictly from the engine.

3.2.2 Steering angle projection and vehicle dynamics

Vehicle coordinate system used in this thesis is shown in Figure [3.1]. It is the conventional right-hand Cartesian coordinate system. The x axis follows from the center of gravity to the front of the vehicle. The y axis goes towards the left side of the car, and z axis lies from the center of gravity to the top of the vehicle. Vehicle's yaw has positive angle increment while turning to the left.

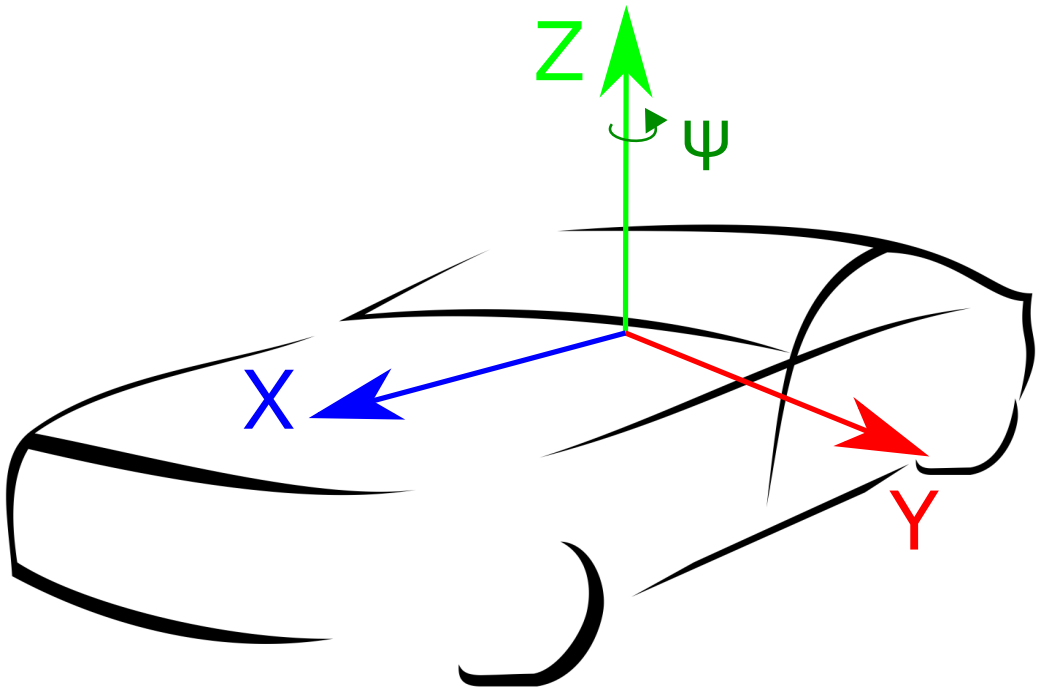

Figure 3.1: The vehicle coordinate system

The single-track model followed the assumptions above is presented in Figure [3.2]. Here, three degrees of freedom exist:

- longitudinal motion

$$-mv(\dot{\beta}+\dot{\psi})\sin\beta + m\dot{v}\cos\beta = F_x; \tag{3.1}$$

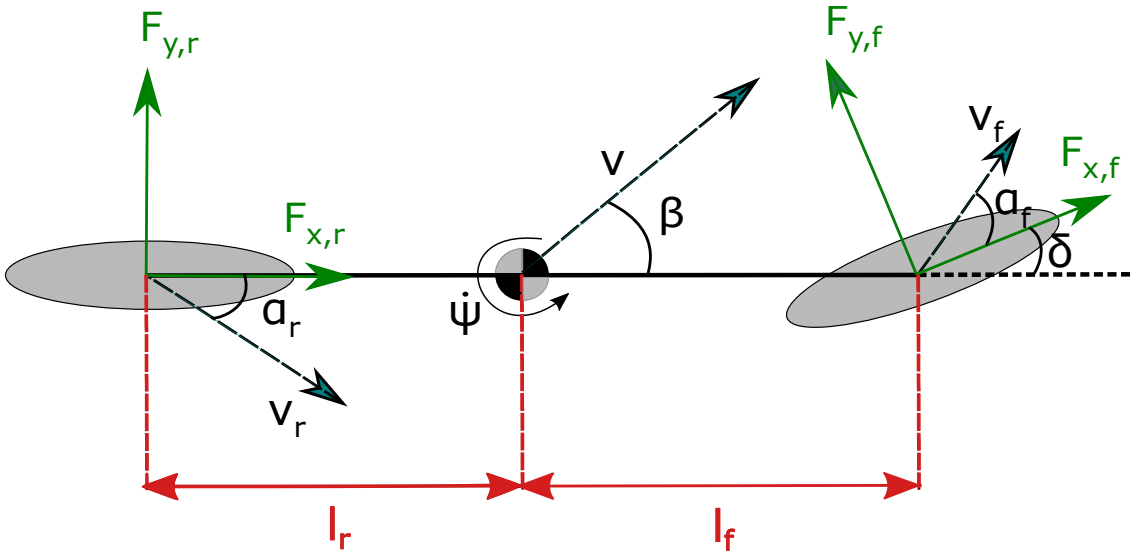

Figure 3.2: The single-track model

- lateral motion

$$-mv(\dot{\beta}+\dot{\psi})\cos\beta + m\dot{v}\sin\beta = F_y; \tag{3.2}$$

- yaw motion

$$I_z\ddot{\psi} = M_z. \tag{3.3}$$

Here, m is the vehicle's mass, v is the velocity of the center of gravity of the vehicle, β is the side-slip angle, ψ is the yaw angle, I_z is the moment of inertia of the vehicle around the z axis. On the right-hand side of the equations, there are forces acting on the center of gravity of the vehicle along with x (F_x) and y (F_y) axes and the moment acting around the z axis (M_z).

From the equations above the following matrix equation can be written down:

$$\begin{pmatrix} mv(\dot{\beta}+\dot{\psi}) \\ m\dot{v} \\ I_z\ddot{\psi} \end{pmatrix} = \begin{pmatrix} -\sin\beta & \cos\beta & 0 \\ \cos\beta & \sin\beta & 0 \\ 0 & 0 & 1 \end{pmatrix} \begin{pmatrix} F_x \\ F_y \\ M_z \end{pmatrix}. \tag{3.4}$$

The forcers F_x and F_y together with the moment M_z can be described by the following steering angle projection (also called the force coordinate transformation):

$$\begin{pmatrix} F_x \\ F_y \\ M_z \end{pmatrix} = \begin{pmatrix} \cos\delta & -\sin\delta & 1 & 0 \\ \sin\delta & \cos\delta & 0 & 1 \\ l_f\sin\delta & l_f\cos\delta & 0 & -l_r \end{pmatrix} \begin{pmatrix} F_{xf} \\ F_{yf} \\ F_{xr} \\ F_{yr} \end{pmatrix}, \tag{3.5}$$

where δ is the steering angle, l_f is the distance from the vehicle's center of gravity to the front axle (the front wheel), and l_r is the distance from the vehicle's center of gravity to the rear axle (the rear wheel). Forces F_{yf} and F_{yr} are calculated via Pacejka

Magic formula described in the section [**Tyre Modelling Approaches**]. During this work, the vehicle is assumed to be Rear-wheel drive (RWD), so $F_{xf} = 0$ and F_{xr} is the second input into the system after the steering angle δ.

After simplifications above the resulting system of nonlinear differential equations describes the steering angle projection and vehice dynamics can be written as follows:

$$\begin{aligned}
\dot{\beta} &= -\dot{\psi} + \tfrac{1}{mv}(\cos\beta(F_{yr} + \cos\delta F_{yf}) - \sin\beta(F_{xr} - \sin\delta F_{yf})), \\
\dot{v} &= \tfrac{1}{m}(\sin\beta(F_{yr} + \cos\delta F_{yf}) + \cos\beta(F_{xr} - \sin\delta F_{yf})), \\
\ddot{\psi} &= \tfrac{1}{Iz}(l_f \cos\delta F_{yf} - l_r F_{yr}).
\end{aligned} \tag{3.6}$$

The system (Eq. 3.6) has two inputs: steering angle δ and force acting on rear tire along x axis F_{xr}. Also, it has three states: the side-slip β, vehicle's centre of gravity velocity v, and it's yaw rate $\dot{\psi}$.

3.2.3 Kinematics

The kinematics of the single-track vehicle model includes calculation of the tires' side-slip angles. Those angles are used in Pacejka Magic formula for calculation of the side tires' forces F_{yr} and F_{yf}. The calculation of tires' sleep angles takes into accaunt the steering angle δ, side-slip angle β, velocity of the center of gravity of the vehicle v, and the yaw rate $\dot{\psi}$ as (formulas are taken from dimploma thetis made by Martin Mondek [6]:

$$\alpha_f = \delta - \arctan\left(\frac{v\sin\beta + l_f\dot{\psi}}{v\cos\beta}\right), \tag{3.7}$$

$$\alpha_r = -\arctan\left(\frac{v\sin\beta - l_r\dot{\psi}}{v\cos\beta}\right), \tag{3.8}$$

where α_f and α_r are the tire's side-slip angles of the front and rear tires respectively.

3.2.4 Block representation

The block diagram of the nonlinear singe-track model is shown in Figure [3.3].

3.3 Linearized Single-Track Model

Linearization of the single-track model (Eq 3.6) is provided assuming that steering angle δ and side slip β are supposed to be smaller than 10 degrees, thus the first assumption can be used:

$$\sin x \approx x, \qquad \cos x \approx 1. \tag{3.9}$$

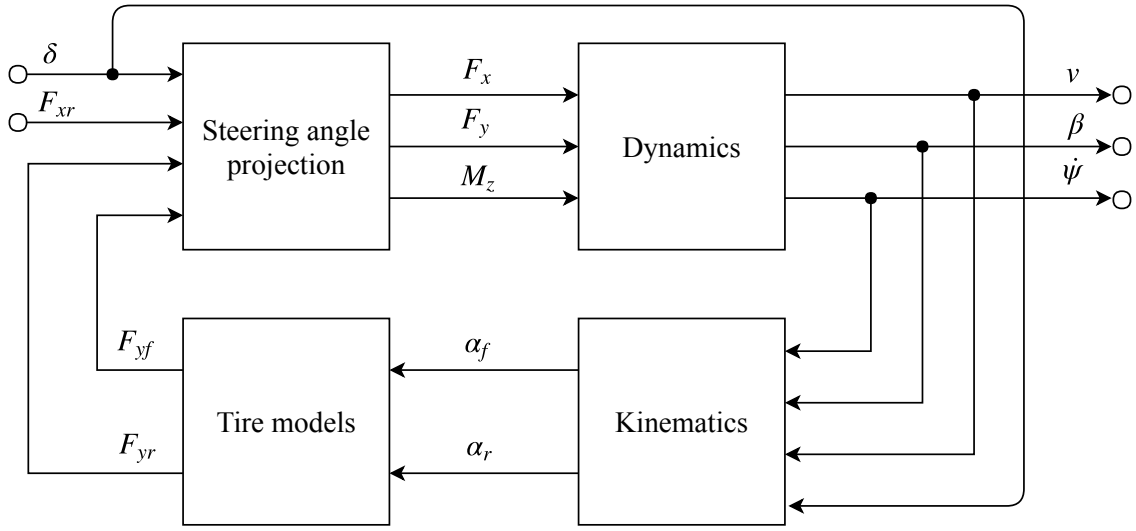

Figure 3.3: The block diagram of the single-track model

With Eq 3.9, the equation 3.6 takes the following form:

$$\begin{pmatrix} mv(\dot{\beta}+\dot{\psi}) \\ m\dot{v} \\ I_z\ddot{\psi} \end{pmatrix} = \begin{pmatrix} -\beta & 1 & 0 \\ 1 & \beta & 0 \\ 0 & 0 & 1 \end{pmatrix} \begin{pmatrix} F_x \\ F_y \\ M_z \end{pmatrix}. \tag{3.10}$$

The velocity is assumed to be constant, thus its derivation is zero $\dot{v} = 0$. The second row yeilds $F_x = -\beta F_y$ and with $\beta^2 \ll 1$ rad. [11] we got:

$$\begin{pmatrix} mv(\dot{\beta}+\dot{\psi}) \\ I_z\ddot{\psi} \end{pmatrix} = \begin{pmatrix} F_y \\ M_z \end{pmatrix}. \tag{3.11}$$

The tire slip angles α_f and α_r can also be linearized as it's done in [6]:

$$\alpha_f = \delta - \beta - \frac{l_f\dot{\psi}}{v}, \tag{3.12}$$

$$\alpha_r = -\beta + \frac{l_r\dot{\psi}}{v}. \tag{3.13}$$

Then lateral forces acting on each tire F_{yf} and F_{yr} can be estimated by linear tire model (Eq. 3.24) as:

$$F_{yf} = C_f\alpha_f = C_f\left(\delta - \beta - \frac{l_f\dot{\psi}}{v}\right), \tag{3.14}$$

$$F_{yr} = C_r\alpha_r = C_r\left(-\beta + \frac{l_r\dot{\psi}}{v}\right), \tag{3.15}$$

where C_f and C_r are cornering stifnesses of the front and rear tires respectivelly.

Now, the lateral forces acting on the vehilce's centre of gravity can be derived from

Eq. 3.5 assuming $F_{xf} = 0$ (the car is assumed to be RWD above) and Eq. 3.9 as:

$$F_y = F_{yr} + F_{yf}. \tag{3.16}$$

Finally, using all assumptions above, the Eq 3.6 takes the following form:

$$\dot{\beta} = -\frac{C_f + C_r}{mv}\beta + \left(\frac{l_r C_r - l_f C_f}{mv^2} - 1\right)\dot{\psi} + \frac{C_f}{mv}\delta, \tag{3.17}$$

$$\ddot{\psi} = \frac{l_r C_r - l_f C_f}{I_z}\beta - \frac{l_f^2 C_f + l_r^2 C_r}{vI_z}\dot{\psi} + \frac{l_f C_f}{I_z}\delta. \tag{3.18}$$

The state-space representation now can be written in matrix form as:

$$\begin{pmatrix}\dot{\beta}\\ \ddot{\psi}\end{pmatrix} = \begin{pmatrix}-\frac{C_f+C_r}{mv} & \frac{l_r C_r - l_f C_f}{mv^2} - 1\\ \frac{l_r C_r - l_f C_f}{I_z} & -\frac{l_f^2 C_f + l_r^2 C_r}{vI_z}\end{pmatrix}\begin{pmatrix}\beta\\ \dot{\psi}\end{pmatrix} + \begin{pmatrix}\frac{C_f}{mv}\\ \frac{l_f C_f}{I_z}\end{pmatrix}\delta. \tag{3.19}$$

Now, the transfer function from the steering wheel δ to the vehicle's yaw rate $\dot{\psi}$ is derived as:

$$G_{\dot{\psi}}(s) = \frac{\dot{\psi}}{\delta} = \frac{b_1 s + b_0}{s^2 + a_1 s + a_0}, \tag{3.20}$$

where coefficients a_0, a_1, b_0, b_1 are:

$$b_0 = \frac{C_f C_r (l_f + l_r)}{I_z m v}, \qquad b_1 = \frac{C_f l_f}{I_z}, \tag{3.21}$$

$$a_0 = \frac{C_f C_r (l_f + l_r)^2}{I_z m v^2} + \frac{C_r l_r - C_f l_f}{I_z}, \qquad a_1 = \frac{C_r + C_f}{mv} + \frac{C_r l_r^2 + C_f l_f^2}{I_z v}. \tag{3.22}$$

The derived transfer function is the same as in [4], this fact allows using conclusion made in the article above, what is provided in the Chapter [**Laterally Unstable Vehicle**].

3.4 Tyre Modelling Approaches

The tire dynamics have a significant impact on the whole vehicle dynamics [7]. There exist a lot of different techniques, which are used to estimate forces and torques, which are generated by tires. Those models are correctly described and compared by Lukas Haffner in [7]. In this work, only two models described below are used.

3.4.1 Pacejka Magic Formula

The most famous tire model is proposed by Hans Bastiaan Pacejka [8], and it considers more than 20 different coefficients. For simplification, he introduced the Simplified Pacejka Magic formula [7], which can be used for estimation not only the the lateral and longitudinal forces' impact on a tire, but also all the torques acting on a wheel around all axis. It has a straightforward calculation, and the same formula is used to

estimate all the forces and torques using different sets of coefficients.

The general Simplified Pacejka Magic formula has the following equation:

$$F(\alpha) = DF_z \sin(C \arctan(B\alpha - E(B\alpha - \arctan(B\alpha)))), \tag{3.23}$$

where D, C, B, and E is the set of shaping coefficients, F_z is a wheel-load, α is a tire's slip-angle (in case of F_x the normalized slip is used), F is an estimated force or torque.

As it is mentioned above, in section [**Nonlinear Single-Track Model**], in this work only the lateral forces F_y (Figure [3.4]) produced by tires are considered. And, as it is described in the chapter [**Force Feedback**], the aligning torque M_z (Figure [3.5]) is used for calculating the force feedback applied by simulator on the steering wheel.

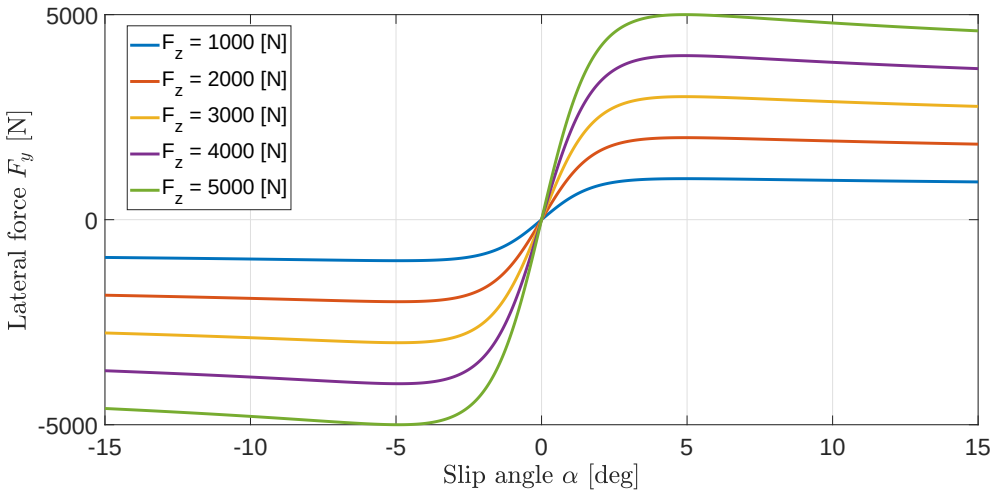

Figure 3.4: Dependence of generated lateral force F_y on tire slip-angle α with different loads F_z

3.4.2 Two-Lines Tire Model

In [12] a simple tire model is utilized. This model contains three parts: two horizontal saturations and one linear part which is a linear approximation of the tire force around zero tire slip angle (or slip ratio in case of longitudinal force)(Figure 3.6). The model equation looks like:

$$F = \begin{cases} C\alpha & |\alpha| < \frac{\mu_{max}}{C}, \\ \mu_{max} & |\alpha| \geq \frac{\mu_{max}}{C}. \end{cases} \tag{3.24}$$

The parameter μ_{max} is a maximal friction coefficient, C is a cornering stiffness in case of F_y (or tire slip coefficient in case of F_x). The equation works for a tire's slip angle α in case of a lateral force F_y or for a tire's slip ratio λ in case of longitudinal force F_x.

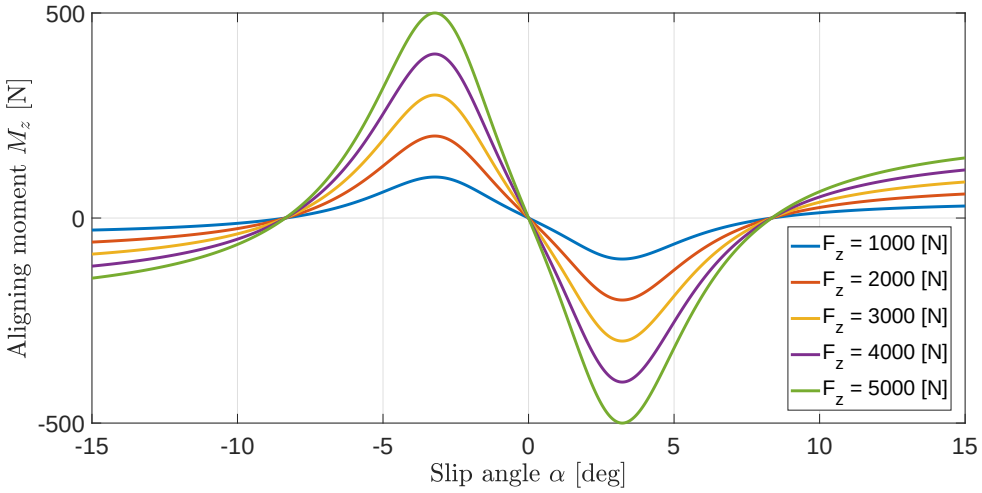

Figure 3.5: Dependence of generated aligning moment M_z on tire slip-angle α with different loads F_z

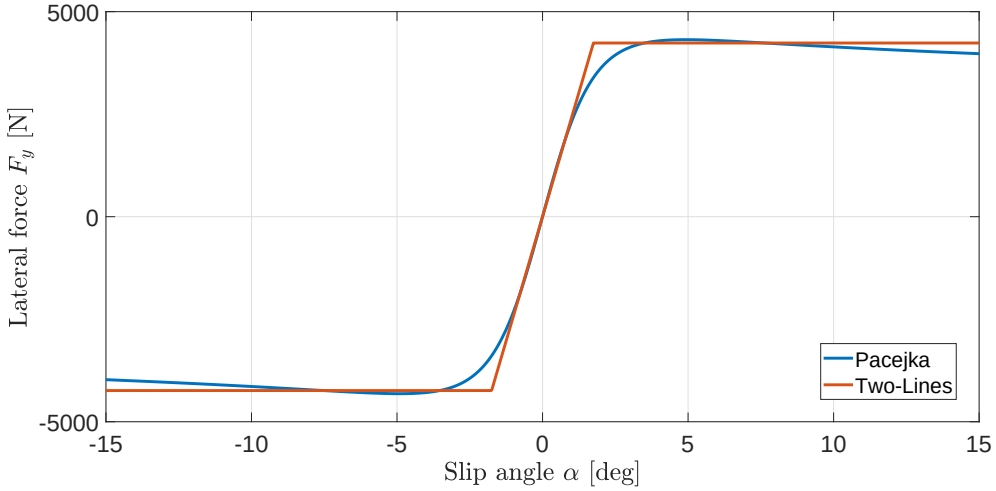

Figure 3.6: Compirison of Pacejka and Two-Lines tire models

4. Laterally Unstable Vehicle

This chapter answers a question: "What is exactly an unstable car?" And the following question: "What it exactly brings to automotive and what is a price?"

The chapter is separated into 4 sections: the section [**Definition of Laterally Unstable Vehicle**] defines the unstable car via existing nomenclature used in automotive; the section [**Critical Velocity**] describes the key parameter of an unstable car; the section [**Practical Meaning of Lateral Instability**] shows the physics behind this term, and the last section [**Pros & Cons of Unstable Vehicles**] summarises the positive and negative factors of making vehicles to be laterally unstable.

4.1 Definition of Laterally Unstable Vehicle

According to Society of Automotive Engineers (SAE) [13], in vehicle dynamics, there are two terms that describe the sensitivity of a car to steering: understeering and oversteering.

Undesteer occurs when a car steers less than angle commanded by the driver, on the other hand, oversteer occures in the case when a car steers more than amount commanded by the driver. Both cases are defined for steady-state cornering where the vehicle follows the constant-path at a constant speed and with a constant steering angle, on a flat surface. The comparison of understeer and oversteer car is shown in Figure 4.1.

The precise definition in [13] is provided via understeer gradient K as:

- when $K > 0$ a vehicle is understeering;
- when $K = 0$ a vehicle is neutral steering;
- when $K < 0$ a vehicle is oversteering.

According to [14] the understeer gradient is defined as a derivative of the front tires' average steer angle with respect to the lateral acceleration imposed to the vehicle at its center of gravity. Figure 4.2 shows an example of its dependency. Reference to [14], the understeer gradient can be calculated as:

$$K = \left(\frac{l_r}{C_f} - \frac{l_f}{C_r} \right) \frac{m}{2(l_f + l_r)}, \tag{4.1}$$

where l_r (l_f) is distance from rear (front) axle to the vehicle's center of gravity; C_r (C_f) is a rear (front) tire's cornering stifness coefficient, and m is vehicle's mass.

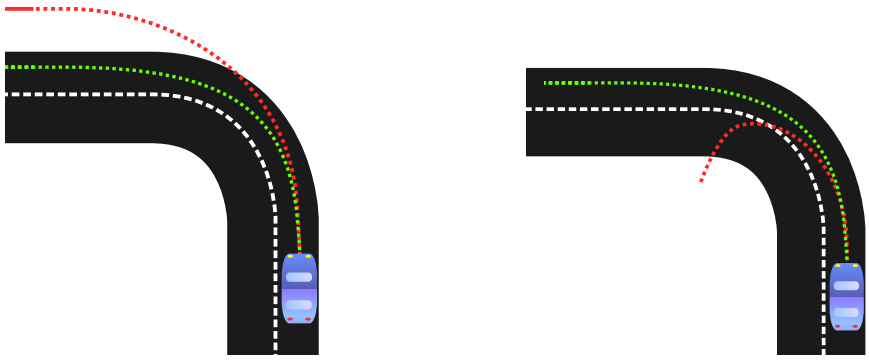

(a) Understeering car cornering. (b) Oversteering car cornering.

Figure 4.1: Comparison of understeering and oversteering car. Images are taken from *https://en.wikipedia.org*. Green path is an optimal cornering trajectory. Understeer: the car goes not turn enough and leave the road. Oversteer: the car turns more sharply and could get to spin.

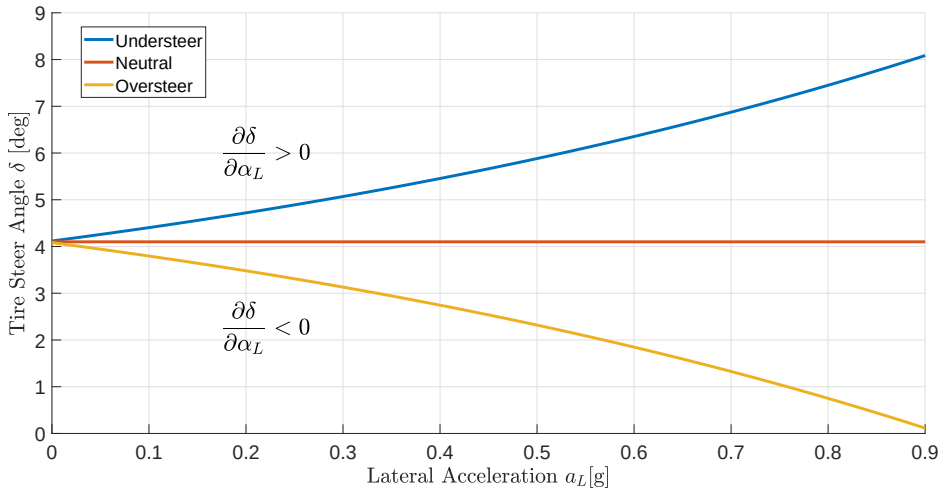

Figure 4.2: Understeer and oversteer definition

It is obvious that $\frac{m}{2(l_f+l_r)}$ is always positive. Thus the sign of the understeer gradient K depends only on the sign of the equation:

$$\text{sign}(K) = \text{sign}(l_r C_r - l_f C_f). \tag{4.2}$$

Therefore, in this work the following definitions are used:

- A vehicle is understeering when $l_r C_r - l_f C_f > 0$;
- A vehicle is neutral steering when $l_r C_r = l_f C_f$;
- A vehicle is oversteering when $l_r C_r - l_f C_f < 0$.

According to [4], Long Wang and Jurgen Ackermann call understeering cars in manner of automatic control engineers as always stable (means that poles of the open loop of the Eq. 3.20 are on the left-half plane for all possible velocities of the vehicle's

center of gravity $v > 0$); and oversteering cars as unstable, because those transfer functions can have unstable poles, and it depends on vehicle's velocity (its dependences is discussed in the next section [**Critical Velocity**]). In this work understeering vehicle can be named as stable vehicle and oversteering as unstable. The neutral steering car can be named as metastable.

4.2 Critical Velocity

According to [4] and [6], the understeering car is always stable, and it has no restriction on critical velocity, because of parameter a_0 from Eq. 3.20 is always greater then 0 in case when $l_r C_r - l_f C_f > 0$. The Figure 4.3 shows changing poles' location of Eq. 3.20 regarding to different velocities in case of understeering car.

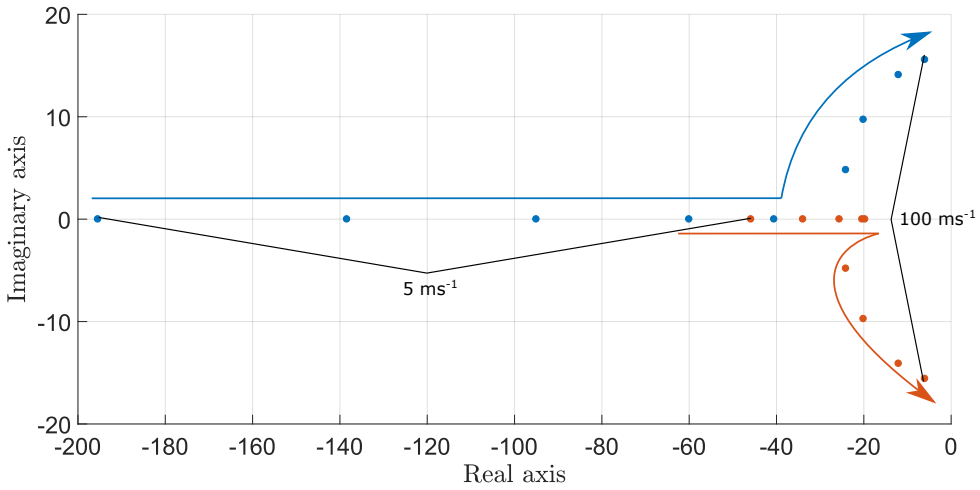

Figure 4.3: Poles location of Eq. 3.20 for understeering car depended on different vehicle's velocities. Arrows show the direction of poles allocation with higher velocity. Car's parameters: $l_f = 1.11$ m, $l_r = 1.89$ m, $C_f = 138820$ N·rad^{-1}, $C_r = 236620$ N·rad^{-1}, $m = 1190$ kg, $I_z = 1141$ kg·m^{-2}.

But, is a case of oversteering car, when $l_r C_r - l_f C_f < 0$, the a_0 can be less than 0, what sets one pole to the right-half plane, and a vehicle becomes unstable on higher velocities. The border of stability of such car is defined as a critical speed v_{crit}. An oversteering car has unstable lateral characteristics when its velocity of the center of gravity v is higher than its critical velocity, which is defined as:

$$v_{crit} = (l_f + l_r)\sqrt{\frac{C_f C_r}{m(C_f l_f - C_r l_r)}}. \tag{4.3}$$

The Figure 4.4 ilustrates the changing poles' location of the transfer function (Eq. 3.20) for a laterally unstable car. The example of stability and instability of the same vehicle is presented in Figure 4.5, where its path on different velocities is shown. When the car goes over its critical velocity, it gets to spin.

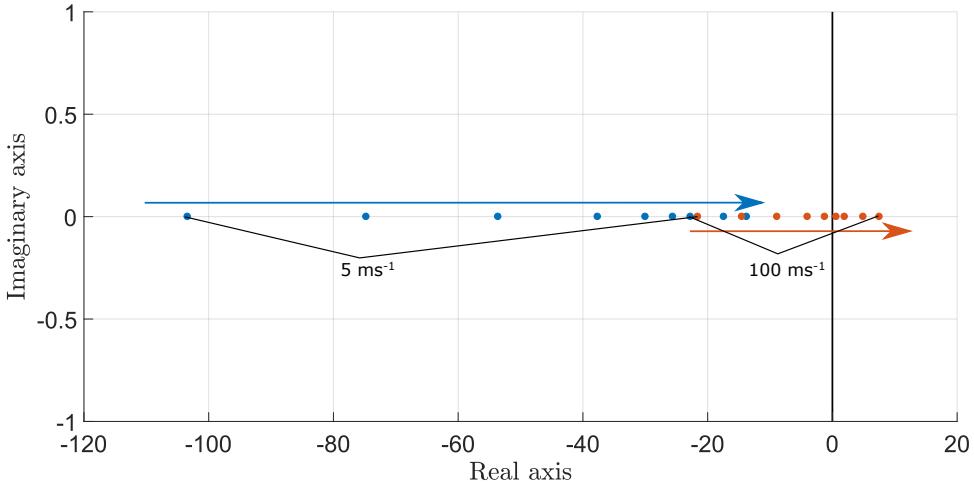

Figure 4.4: Poles location of Eq. 3.20 for oversteering car depended on different vehicle's velocities. Arrows show the direction of poles allocation with higher velocity. Car's parameters: $l_f = 2.07$ m, $l_r = 0.93$ m, $C_f = 258700$ N·rad^{-1}, $C_r = 116730$ N·rad^{-1}, $m = 1190$ kg, $I_z = 3900$ kg·m^{-2}. In this case $v_{crit} \approx 23$ m·s^{-1}.

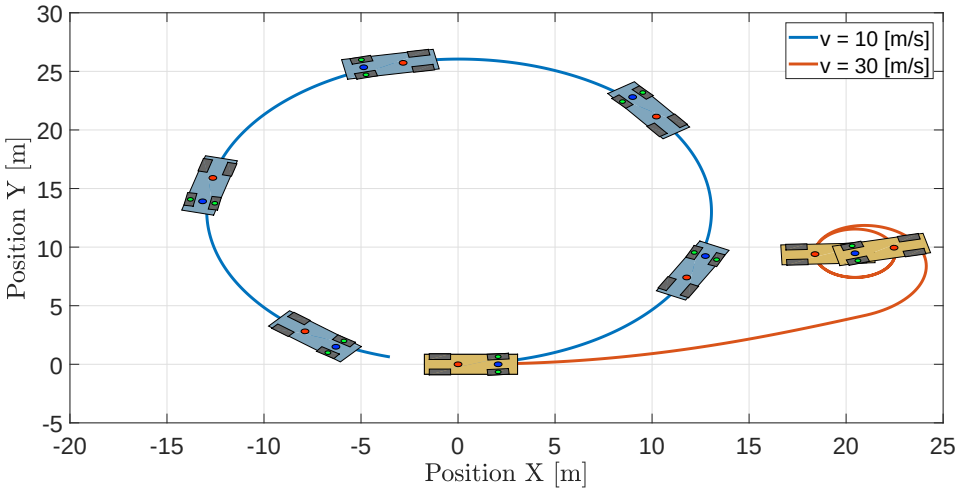

Figure 4.5: Paths of the same vehicle on the different velocities, steering angle $\delta = 0.2$ rad. Cars are plotted every 1.5 s. Car's parameters are the same as in the Figure 4.4. In this case $v_{crit} \approx 23$ m·s^{-1}. *(For the path generation a plotting function created by M.Mondek in [6] was used.)*

More about critical speed and its dependencies on all parameters can be seen in [6].

In provided tests, there appeared an issue with the defference of theoretically calculated critical velocity derived within analyzes of the linear model and critical velocity observed on the nonlinear model. These velocities do not match and typically, the theoretical calculated value is greater than value estimated by observation ($v_{crit,lin} \approx 23$ m·s^{-1} versus $v_{crit,nonlin} \approx 12$ m·s^{-1} in case of the car with parameters from the Figure [4.4]). This fact leads to using robust design methods for creating regulators for real ground vehicles. This statement must be checked in future works.

4.3 Practical Meaning of Lateral Instability

The main difference between understeering and oversteering cars is that during cornering maneuver the first one has grater slip angle's on both tires. Hence, the practical meaning of lateral instability is pretty simple: unstable vehicle doing a cornering maneuver at a velocity greater than its critical speed can get a spin. This is the main problem and general reason, why automotive companies are producing common consumer cars as understeering. Let it be less agile, but don't let it get a spin doing lateral maneuvers.

The Figures 4.6 and 4.7 show a comparison of tires' slip angels of the same unstable vehicle at different velocities. It can be seen that when an unstable vehicle goes on velocity greater than critical, the sum of slip angles of both tires grows dramatically. In comparison, when the same car goes on velocity less than its critical, the sum is $\alpha_f + \alpha_r \approx 0$.

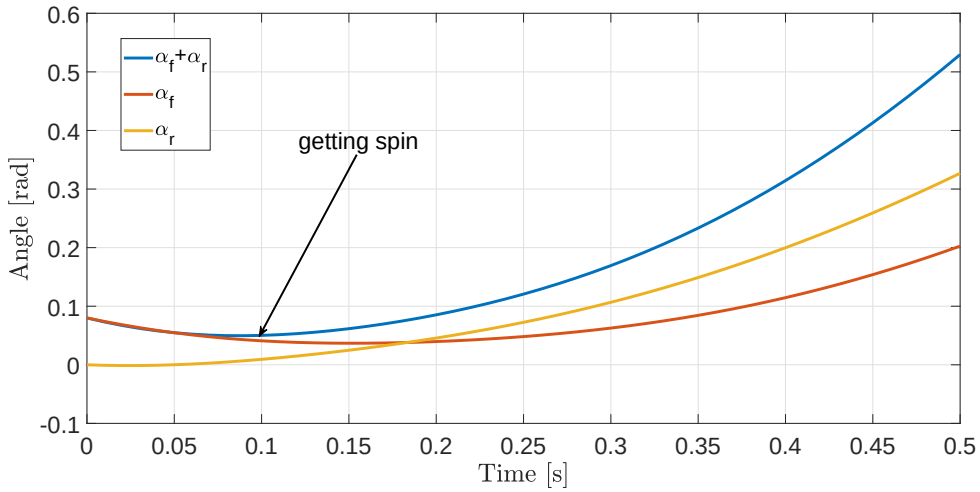

Figure 4.6: Tires' slip angles during cornering maneuver $v = 25$ m s^{-1}, $\delta = 0.08$ rad (≈ 4.5 deg) of unstable vehicle with parameters as in Figure 4.4

4.4 Pros & Cons of Unstable Vehicles

There are several profits of making vehicles laterally unstable, however, there are costs to be paid. All of the pros and cons of oversteering cars are listed below.

Laterally unstable vehicles have the following pros:

- An oversteering car is agiler: in steady-state cornering maneuver, it always will have yaw rate higher than the same but understeering car. The Figure 4.8 visu-

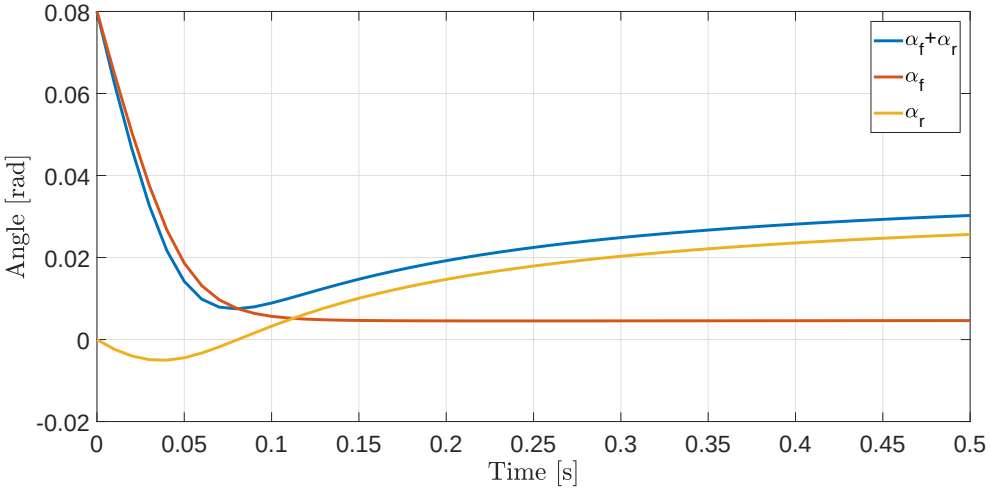

Figure 4.7: Tires' slip angles during cornering maneuver $v = 10$ m s^{-1}, $\delta = 0.08$ rad (≈ 4.5 deg). Vehicle parameters are the same as in Figure 4.4

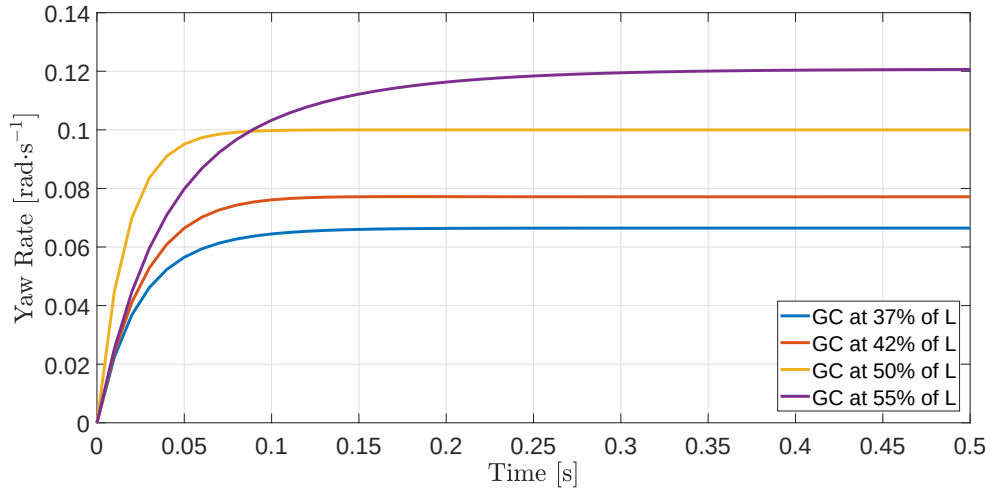

Figure 4.8: Yaw rate of the vehicle with $m = 1190$ kg, $L = l_f + l_r = 3$ m. Steering angle $\delta = 0.01$ rad., velocity $v = 30$ m·s^{-1}. Cars with GC (gravity center) equals to 37, and 42 percent are understeering; 50 - neutral steering; and 55 - oversteering.

alizes yaw rate of the same vehicle (with the changed center of gravity location) doing the same cornering maneuver.

- Rear wing used for lateral stabilization on higher velocities can be eliminated. That reduces the aerodynamic drag of a vehicle and as the primary result, it saves energy to spend on its drag. The chapter [**Simulation Tests**] overviews among other things, this option.

- And the main advantage is that as it is shown in [14], yaw rates feedback to the front wheel steering angle by a positive PID controller cannot destabilize oversteering cars below their critical velocity. At the same time, for understeering cars, there is a possibility of destabilization (condition is derived in [14]). This feedback is the central part of all proposed regulators listed below in the chapter

[**Proposed Control Architectures**].

Lateral instability brings the following cons:

- The necessity of regulation of the whole steering system arises [4].
- For part of the proposed regulators, tire's slip angles α_f and α_r or side-slip β should be estimated, because there is no possibility of direct measure exists. The overview of existing estimators is presented in the chapter [**Slip Estimation Algoritms**].
- Using regulation, we get a steer-by-wire vehicle. This problematic is considered below in the chapter [**Force Feedback**].

5. Proposed Control Architectures

This chapter describes proposed regulation architectures, which are then tested in the chapter [**Simulation Tests**]. Root locus characteristics of all controllers are shown on a vehicle with parameters from the Figure 4.4, which is slightly unstable and has critical velocity $v_{crit} \approx 50$ m·s^{-1}.

Section [**Yaw Rate Tracking**] describes basis control approach, sections [**Augmented Yaw Rate Tracking: Side-slip and Steering Angle Control**] and [**Augmented Yaw Rate Tracking: Tire's Slip Sum**] show its possible augmentation. Section [**Conclusion**] lists possibilities for making the regulation better.

5.1 Yaw Rate Tracking

This control technique is a basis for each type of the following regulators. It is based on the idea described by Long Wang and Jurgen Ackermann in [11]. In this article, the possibility of control by positive PID regulator on feedback from the yaw rate to the steering angle is described. Especially, they conclude that this type of regulator cannot destabilize the oversteering car moving over its critical velocity.

The transfer function from the steering angle to the yaw rate is (Eq 3.20). The diagram in Figure 5.1 shows the regulator signal flow. On the integrator suitable anti-wind-up saturation should be applied. The whole output goes through saturation block which means maximum possible steering angle is set to the front axle.

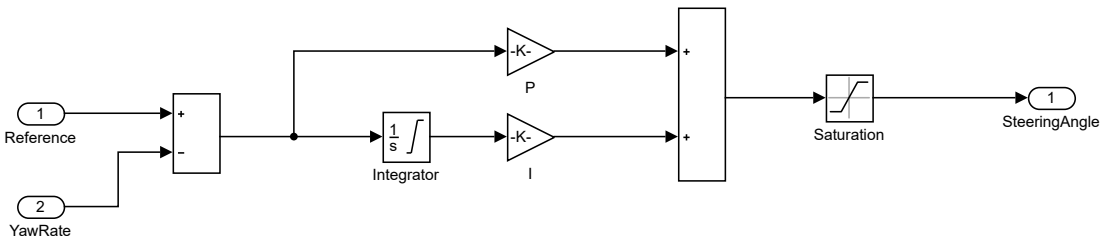

Figure 5.1: Diagram of yaw rate tracking control.

For creating the regulator, root locus technique was used. The Figure 5.2 presents the root locus of a closed loop system for an oversteering car with PI controller. In Figure 4.4 the location of the poles of an open loop system is presented. As we can see, there is no oscillation characteristic. Therefore, in a closed loop, poles are set to the real axis to save vehicle's native dynamics.

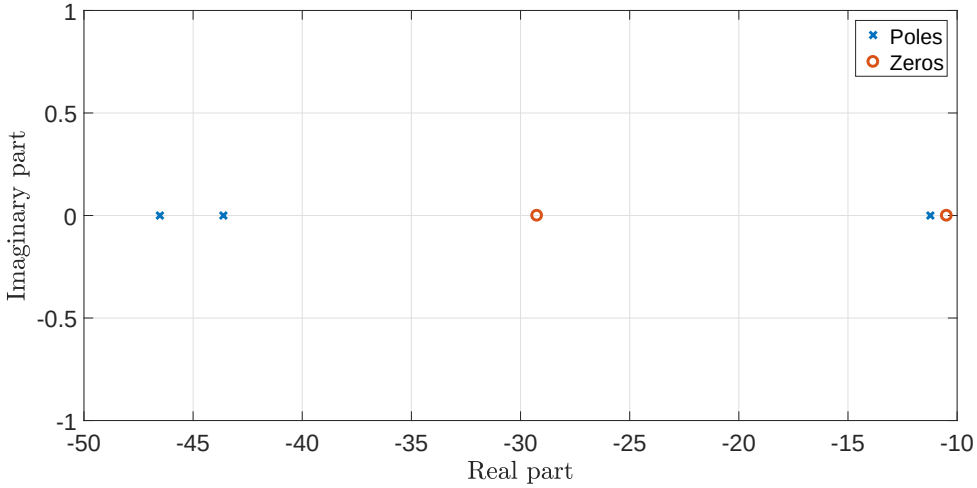

Figure 5.2: Root locus of the closed system at $v = 50$ m·s^{-1}.

5.2 Augmented Yaw Rate Tracking: Side-slip and Steering Angle Control

This control technique uses yaw rate reference and current velocity to calculate references for side-slip and steering angles, and positive P regulators to reach the references in internal loops. Experimental simulation tests showed that the anti-wind-up saturations for the external yaw rate tracking loop can be compromised.

For the calculation of the set points for side-slip and steering angles linearized single-track model (Eq. 3.19) was used:

$$\delta_{ref} = \frac{a_{11}a_{22}\dot{\psi}_{ref} - a_{21}a_{12}\dot{\psi}_{ref}}{a_{21}b_1 - a_{11}b_2}, \tag{5.1}$$

$$\beta_{ref} = \frac{b_1\delta_{ref} - a_{12}\dot{\psi}_{ref}}{a_{11}}, \tag{5.2}$$

where $a_{i,j}$, $i, j \in \{1, 2\}$ are coefficients of the matrix A, and b_i, $i \in \{1, 2\}$ are coefficients of the matrix B of the linearized single-track model (Eq. 3.19).

The transfer function from the steering angle to the side-slip angle is:

$$G(s) = \frac{\beta(s)}{\delta(s)} = \frac{b_1 s + b_0}{s^2 + a_1 s + a_0}, \tag{5.3}$$

where coefficients a_0, a_1, b_0, b_1 are:

$$b_0 = \frac{C_f C_r l_r (l_f l_r)}{m v^2 I_z} - 1, \qquad b_1 = \frac{C_f}{mv}, \tag{5.4}$$

$$a_0 = \frac{C_f C_r (l_f + l_r)^2}{I_z m v^2} + \frac{C_r l_r - C_f l_f}{I_z}, \qquad a_1 = \frac{C_r + C_f}{mv} + \frac{C_r l_r^2 + C_f l_f^2}{I_z v}. \tag{5.5}$$

The Figure 5.3 presents the changing of pole location within introducing of the closed loop with feedback from the steering angle to side-slip angle.

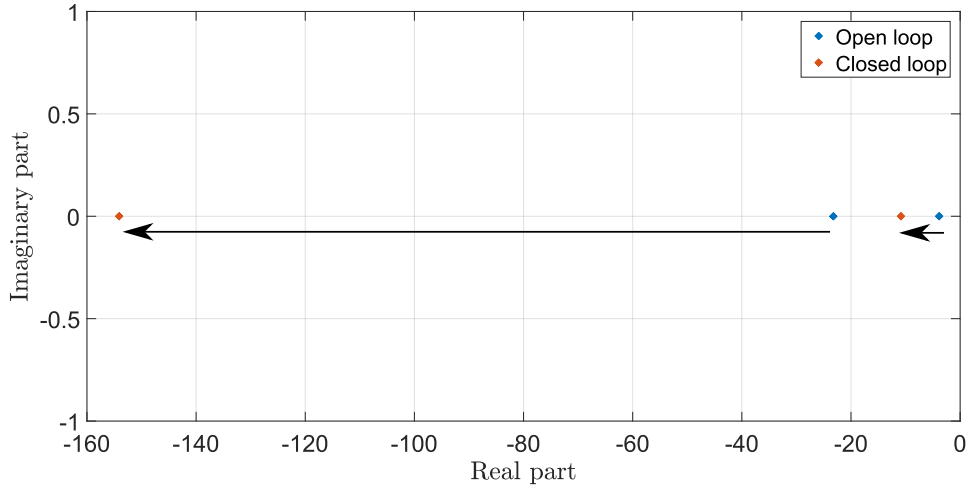

Figure 5.3: Changing of pole location by side-slip damper for unstable car at $v = 50$ m·s^{-1}.

The Figure 5.4 shows a diagram of signal flow in the controller.

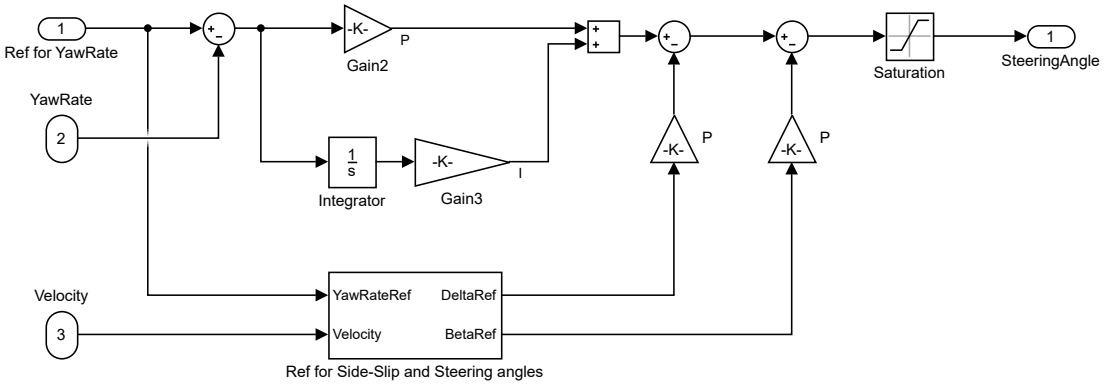

Figure 5.4: Diagram of augmented yaw rate tracking control with the addition of side-slip and steering angles control.

5.3 Augmented Yaw Rate Tracking: Tire's Slip Sum

This control technique uses the sum of tire's slip angles for creating of an artificial border for maximum possible yaw rate on high velocities. The simulation model equipped with this type of controller did not get to a spin situation (that caused to other kinds of regulation on a higher speed with keeping a reference for yaw rate on a physical maximum of tested cars). The primary problem of that control architecture is regulation delay about 0.2-0.3 s.

The Figure 5.5 shows an example of bounding on high velocity. In comparison, in Figure 5.6, the behavior of the same control technique on smaller speed is presented.

Also, the small delay in reference tracking can be seen.

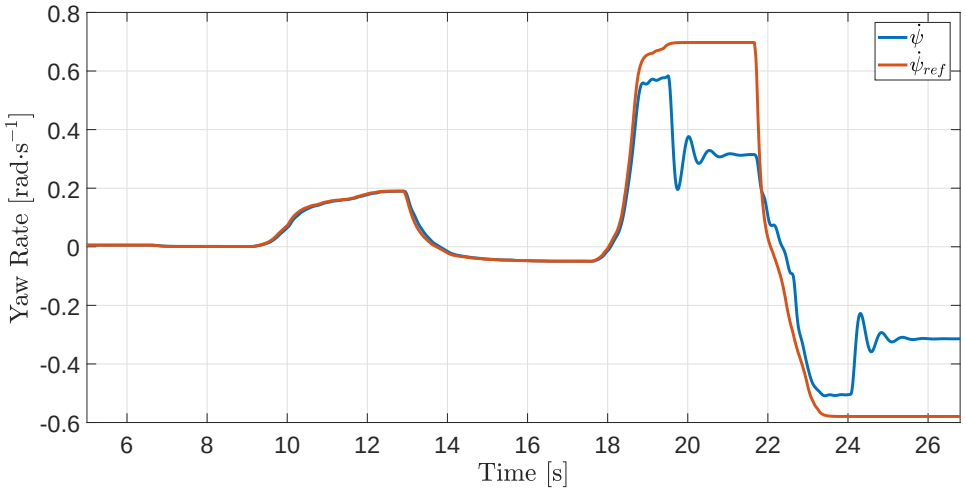

Figure 5.5: The behavior of the regulated unstable car equipped with yaw rate tracking with tire's slip sum damper on velocity $v = 50$ m·s^{-1}. For higher yaw rate references artificial boundness arises.

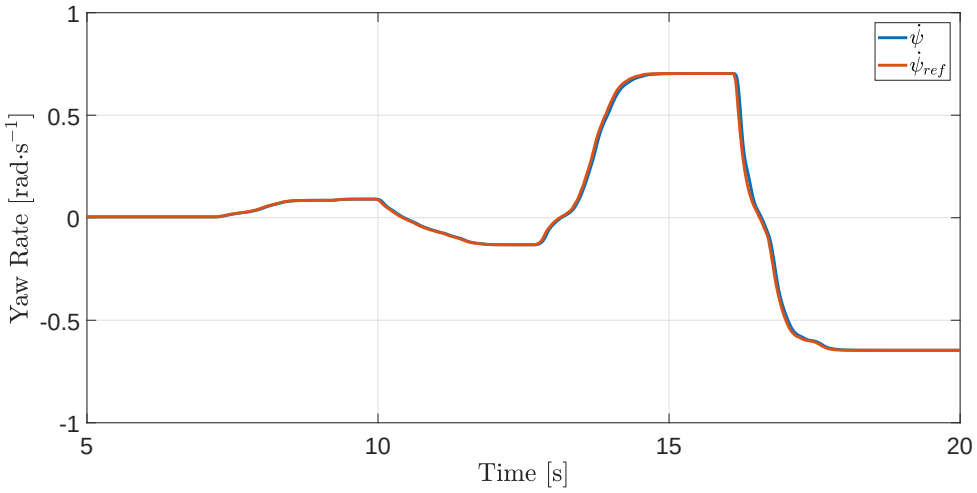

Figure 5.6: The behavior of the regulated unstable car equipped with yaw rate tracking with tire's slip sum damper on velocity $v = 20$ m·s^{-1}. There is no bounding.

The transfer function from the steering angle to tire's slip angles sum is derived from linearized tire's slip angles (Eq. 3.12 and Eq. 3.13):

$$G_{\alpha^+}(s) = \frac{(\alpha_f + \alpha_r)(s)}{\delta(s)} = \mathbb{1}(s) - 2G_\beta(s) + \frac{l_r - l_f}{v} G_{\dot{\psi}}(s), \tag{5.6}$$

The Figure 5.7 presents root locus of the internal closed loop. As can be admitted, it has an unstable zero and pole. Nevertheless, the outer loop keeps the system in the stable zone.

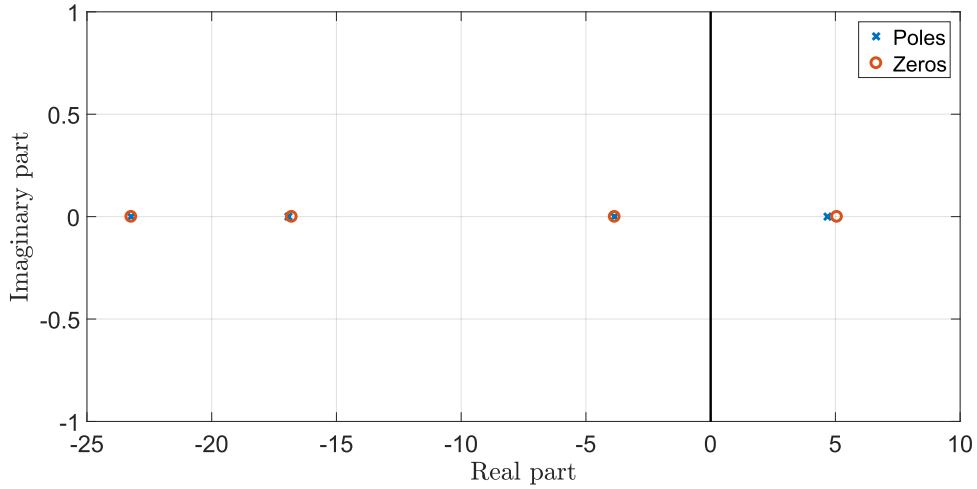

Figure 5.7: Root locus of the internal loop at $v = 50$ m·s^{-1}.

The Figure 5.8 shows a diagram of signal flow for this type of regulation.

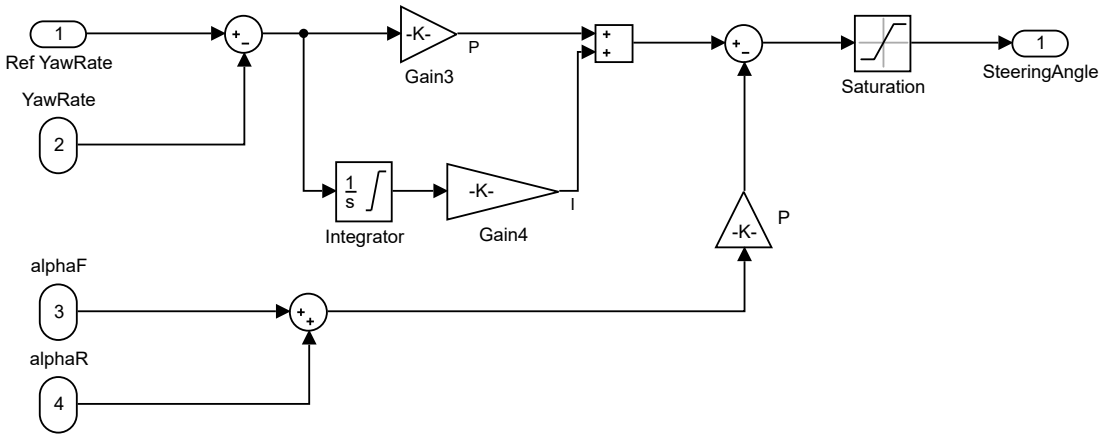

Figure 5.8: Diagram of augmented yaw rate tracking control with the addition of tire's slip angles sum control.

5.4 Conclusion

Proposed controllers stabilize a laterally unstable vehicle, but they can also be used for stable cars. These control techniques are not optimal and robust. There are possibilities of increasing the quality of a regulation: using robust regulation methods (proposed regulators suffer on precise of the linearization); creating a batch of controllers for different velocities; there is a possibility of using state feedback and based on this approach regulation techniques.

Also, for the future work, there are other possibilities of control, which are not described in this thesis: reference tracking in outer loop for tire's slip angles α_f or α_r, or side-slip angle β. Moreover, there is an idea to work with tire's slip difference $\alpha_f - \alpha_r$.

6. Simulation Tests

6.1 Yaw Rate Tracking Test

Yaw rate tracking test branch was the primary test for all regulators before the test on a simulator. It was provided by a non-linear single-track model (Eq. 3.6) with parameters of a vehicle listed under the Figure 4.4. This test branch includes a reference tracking on different velocities and with added noise imitating wind and real road.

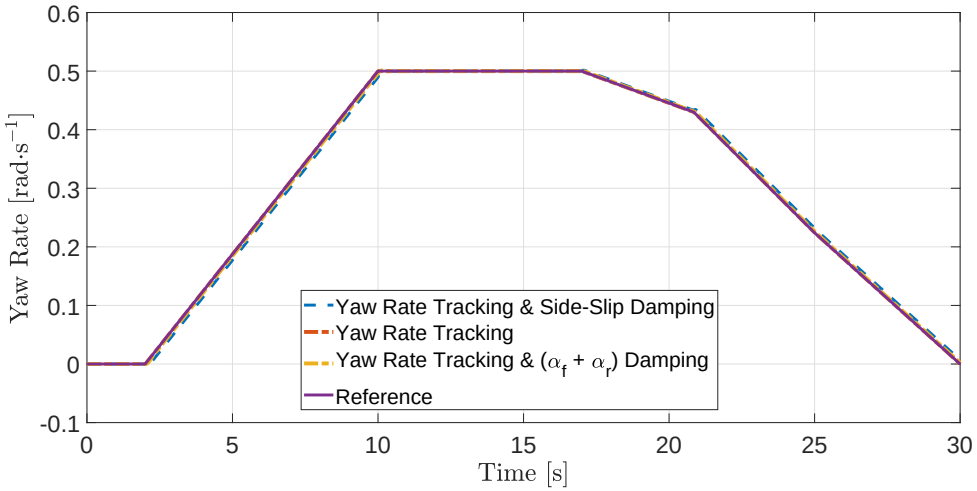

Figure 6.1: Regulator comparison at $v = 10$ m·s^{-1}.

The Figure 6.1 shows a comparison of all regulators on a sufficiently small velocity, at $v = 10$ m·s^{-1}. All of the proposed control techniques work well at a low speed. With a higher (Figure 6.2) velocity ($v = 20$ m·s^{-1}) the main difference between the 3rd controller, which uses the sum of tires' slip angles damper, and others is correctly seen. This regulator keeps side-slip sufficiently small to pretend to get a spin (Figure 6.3). The first two regulators, yaw rate tracker and its augmentation with side-slip reference tracking work well. Nevertheless, as it can be seen in Figure 6.4, its primary problem is that on a non-linear model this regulator cannot prevent a spin situation, that is shown in the next test with a bit higher velocity ($v = 23.5$ m·s^{-1}). After keeping on a high yaw rate reference for a sufficiently long period of time, vehicles got to spin. In comparison, the 3rd controller prevened this situation.

The next Figure 6.5 shows test results including a noise added on side-slip imitating small hummocks on the road and small wind gusts acting on the vehicle. It can be seen that the 3rd regulator does not have an excellent noise suppression. It can be solved by using of a low-pass filter on the inner closed loop, which also brings additional small control delay.

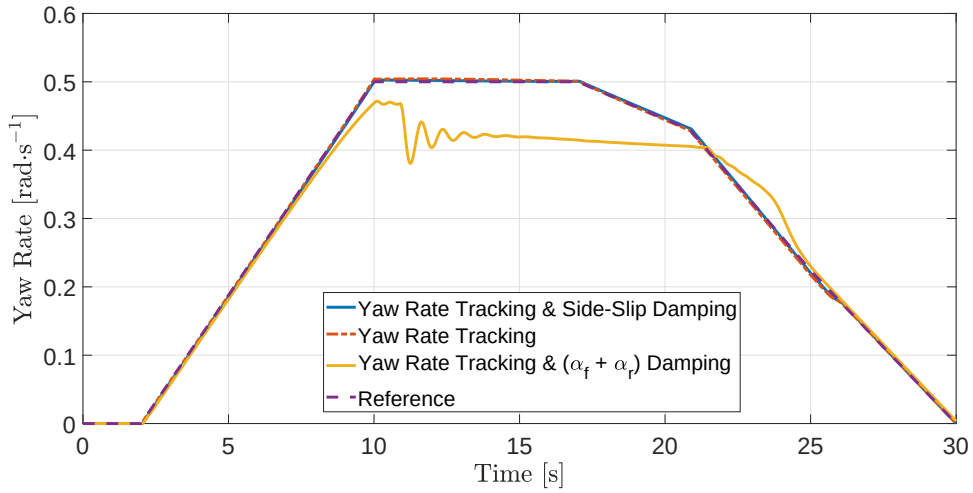

Figure 6.2: Regulator comparison at $v = 20$ m·s^{-1}.

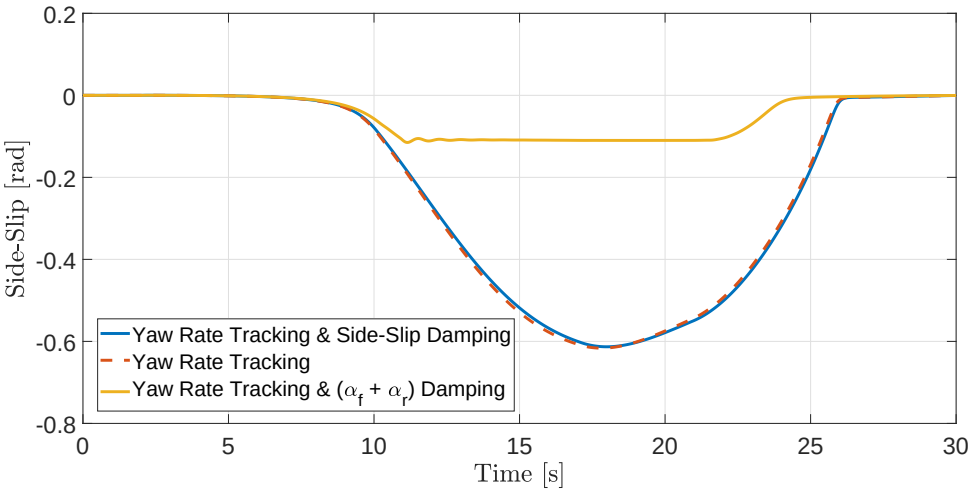

Figure 6.3: Regulator comparison at $v = 20$ m·s^{-1} (Side-slip).

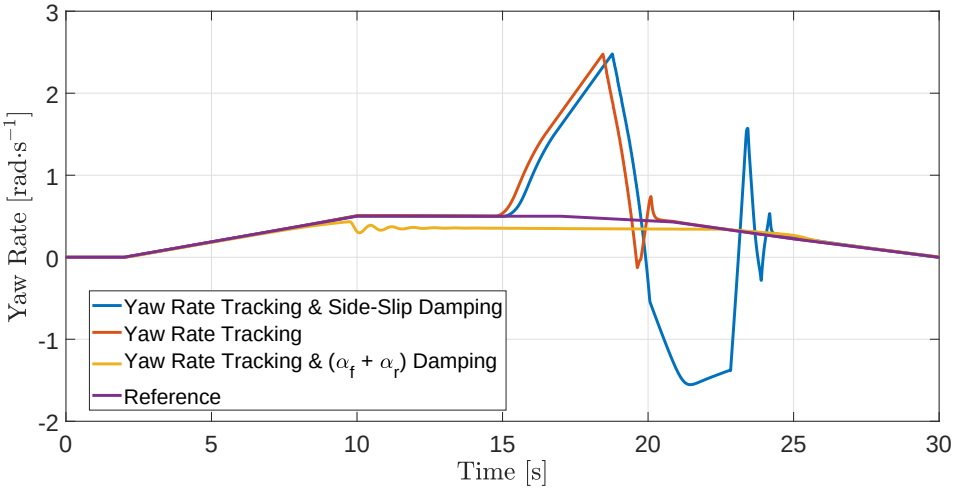

Figure 6.4: Regulator comparison at $v = 23.5$ m·s^{-1}.

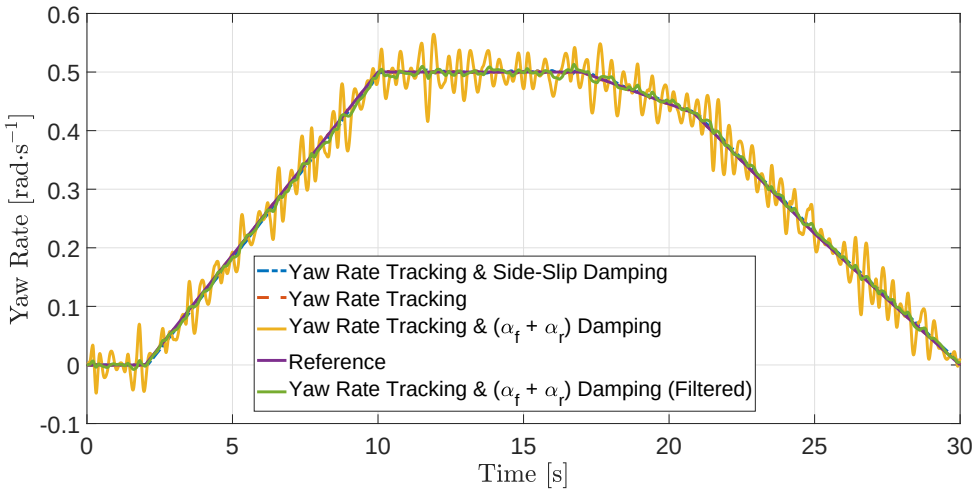

Figure 6.5: Regulator comparison with noise at $v = 15$ m·s^{-1}.

Provided tests correctly show that laterally unstable vehicle can be stabilizable, but with some restrictions. In chapter [**Laterally Unstable Vehicle**] was stated that, according to the linearized model, these types of control techniques could not destabilize an unstable vehicle. But, as it seen, tests provided on a non-linear model shows that there always are some restrictions on a possible physical maximum perfomance of an unstable car. And this restrictions can be solved, for example by using the 3rd regulator, or by introducing of a non-linear analog of the basis regulator.

Nevertheless, results of tests provided on the simulator are optimistic, and they show a possibility of control an unstable vehicle and open a wilder field to discussions.

6.2 Spoiler Elimination

Spoiler or rear wing is used to help a driver handle the car at higher velocities. It produces an anti-lift force that increases the vertical force acting on the rear axle to improve traction and maneuverability (increasing of lateral forces acting on rear tires (Eq. 3.23)). On the other hand, cars equipped with rear wing have higher atmospheric drag, what increase fuel consumption. Creating a rear wing is always a trade-off between generated anti-lift and drag forces. But spoilers can be reduced when a vehicle is equipped with active artificial stabilization. This statement is proven below.

To provide an experimental prove the non-linear single-track model must be augmented by aerodynamic forces acting on a vehicle. These forces can be calculated using the following equation [1]:

$$F = cS\frac{\rho}{2}v^2, \tag{6.1}$$

where F is a calculating force (F_l for anti-lift or F_d for drag); c is an aerodynamic con-

stant (c_l for anti-lift or c_d for drag); S is an effective cross-sectional area (is assumed to be constant); ρ is the air density; v is an air velocity (is assumed to be equal to the vehicle's velocity).

The augmented non-linear single-track model takes the following form:

$$\begin{aligned}
\dot{\beta} &= -\dot{\psi} + \tfrac{1}{mv}(\cos\beta(F_{yr}(F_{zr}+F_l)+\cos\delta F_{yf}) - \sin\beta(F_{xr}-F_d-\sin\delta F_{yf})),\\
\dot{v} &= \tfrac{1}{m}(\sin\beta(F_{yr}(F_{zr}+F_l)+\cos\delta F_{yf}) + \cos\beta(F_{xr}-F_d-\sin\delta F_{yf})),\\
\ddot{\psi} &= \tfrac{1}{Iz}(l_f\cos\delta F_{yf} - l_r F_{yr}(F_{zr}+F_l)),
\end{aligned} \tag{6.2}$$

where lateral force acting on a rear wheel $F_{yr}(F_{zr}+F_l)$ is now a function of the sum of vertical forces acting on the rear axle (gravity and anti-lift). Gravity force is constant; only anti-lift force is changed. Also, drag is a dissipative force acting on a rear axle in a longitudinal direction.

For this test, the same slightly unstable car is used (with parameters listed under the Figure 4.4). Three cars are tested: the vehicle without stabilization, the vehicle equipped with yaw rate tracking controller, and the vehicle equipped with the rear wing. Coefficients c_d (0.36 for car with rear wing and 0.31 for cars without it) and c_l (0.26 only for car with rear wing) are taken from [17]. S is assumed to be 1 (in case of rear wing) and 8 (in case of a whole car).

The Figures 6.6 and 6.7 show the comparison between yaw rate and additional force applied by cruise control on vehicle models in a test with applied step with attitude 0.02 rad on side-slip angle β, what imitates a bump or wind gust. It can be correctly seen that the vehicle equipped with controller keeps zero yaw rate better than the car equipped with the rear wing. Moreover, the reduced drag also reduces the force applied to the rear axle to keep the desired velocity.

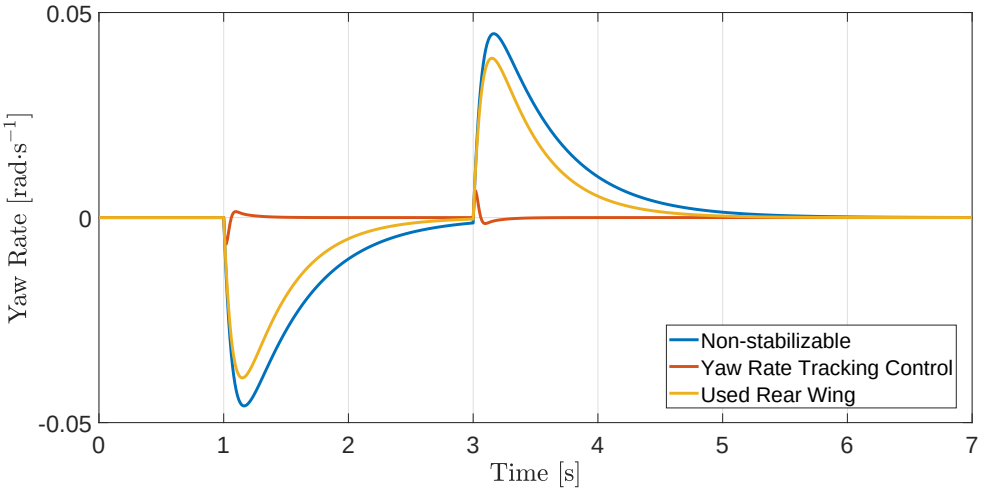

Figure 6.6: Comparison of a yaw rate of a vehicle with applied wind gust at a velocity $v = 40$ m·s^{-1}.

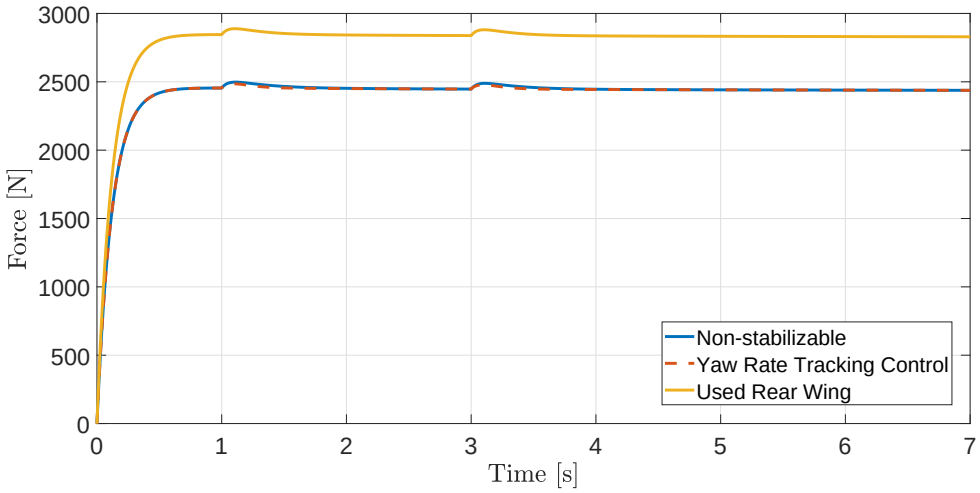

Figure 6.7: Comparison of applied longitudinal force on the rear wheel by cruise control with applied wind gust at velocity $v = 40$ m·s^{-1}.

7. Slip Estimation Algoritms

This chapter is a short overview of a possible measure and estimation techniques that can be used to get a missing parameters' values for proposed control architectures: tire's slip angles and side-slip angle.

7.1 Overview of Tire's Slip Angle Estimators

This section describes primary principles of tire's slip angle estimation. The overview is based on dissertation work by Lukas Haffner [7].

The measurement of tire's slip angle α can be done indirectly by velocity sensors in lateral and longitudinal directions and then applying formulas from vehicle's kinematics (Eq. 3.7 and 3.8 with substituted ratio of longitudinal v_x and lateral v_y velocities for vehicle's side-slip angle β):

$$\alpha_f = \delta - \frac{v_y}{v_x} - \frac{l_f \dot{\psi}}{v_x}, \tag{7.1}$$

$$\alpha_r = -\frac{v_y}{v_x} + \frac{l_r \dot{\psi}}{v_x}. \tag{7.2}$$

This solution is expensive due to a price of velocity sensors, and it is not suitable for mass car production. As an alternative, there exist observer methods.

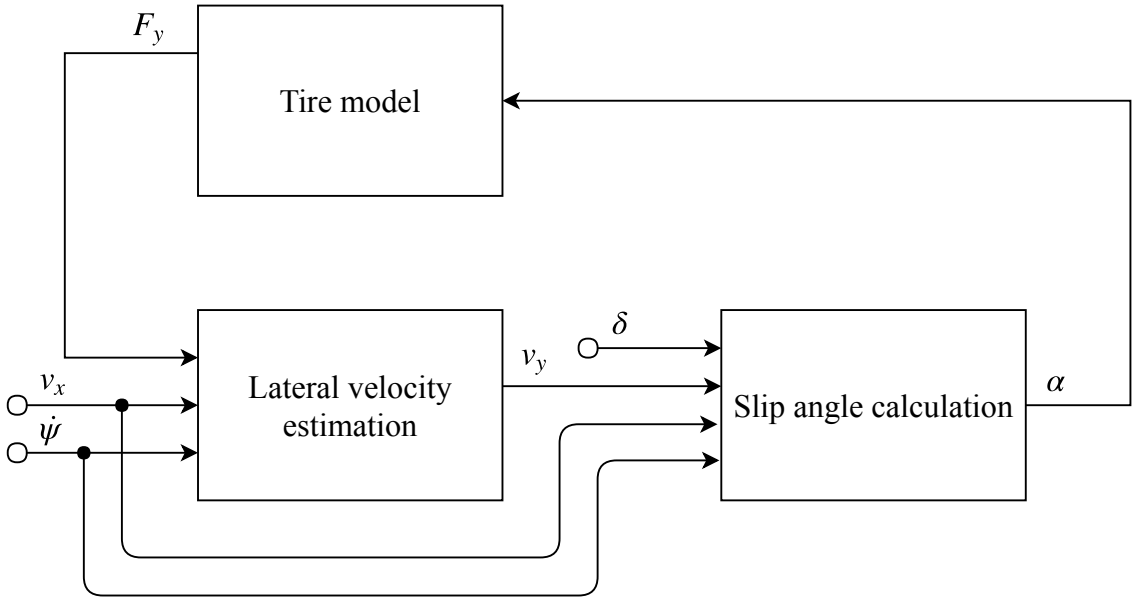

Figure 7.1: Diagram of tire's slip angle estimation

Commonly, they are based on separation principle shown in the Figure 7.1. The estimation is divided into three parts:

- Calculation of lateral tire force F_y by a suitable tire model. Depending on the

desired accuracy, models described in the chapter [**Used Vehicle Modelling Approaches**] or in [7] can be chosen.

- The second block in the diagram refers to a suitable estimation algorithm for reaching a value of a lateral velocity v_x. For estimation there exist two main groups of techniques: Kalman filter (Linear Kalman filter, Extended Kalman filter), and sliding mode observers (such as Utkin observer or Walcott-Żak observer). A comparison of the mentioned estimators is provided in [7].

- The last block in the diagram refers to α-calculation using kinematics formulas (Eq. 7.1 and 7.2).

7.2 Overview of Side-Slip Angle Estimators

In vehicle's side-slip angle measurements there are the same possibilities as well as issues as in the field of tire's slip angle estimation. Namely, there is the same possibility of indirect calculation of the side-slip β from measurements of velocity sensors in lateral and longitudinal directions with applying of kinematic equation [6] and [7]:

$$\beta = \arctan \frac{v_x}{v_y} \approx \frac{v_x}{v_y}. \tag{7.3}$$

But the same problem arises: velocity sensors are expensive. From this fact follows the same solution: use a side-slip estimator.

There exist hundreds of research articles about the estimation of vehicle's side-slip angle, from vehicle dynamics model to neural networks. This overview is based on the idea described in [15]. Generally, the side-slip estimator is implemented via tires' slip angles estimation algorithms. The diagram in Figure [7.2] shows commonly used separation signal flow:

- The first block, tires' slip angles estimator means the estimator described above in the section [**Overview of Tire's Slip Angle Estimators**]. The output of this block is tires' slip angles and lateral velocity of each wheel.

- The second block represents tires' slip ratios calculation using the formula (Eq. 7.4).

- The third block calculates lateral and longitudinal forces generated on each wheel via suitable tire's model. Slip ratio λ of each tire is used to calculate longitudinal forces generated by that wheel, and slip angle α is used for calculation of lateral force.

- The last block uses the internal state and its inputs to estimate by suitable method (as an example Extended Kalman filter) the vehicle's side-slip angle β. The used formula can be taken from the nonlinear single-track model. (first equation from Eq. 3.6)

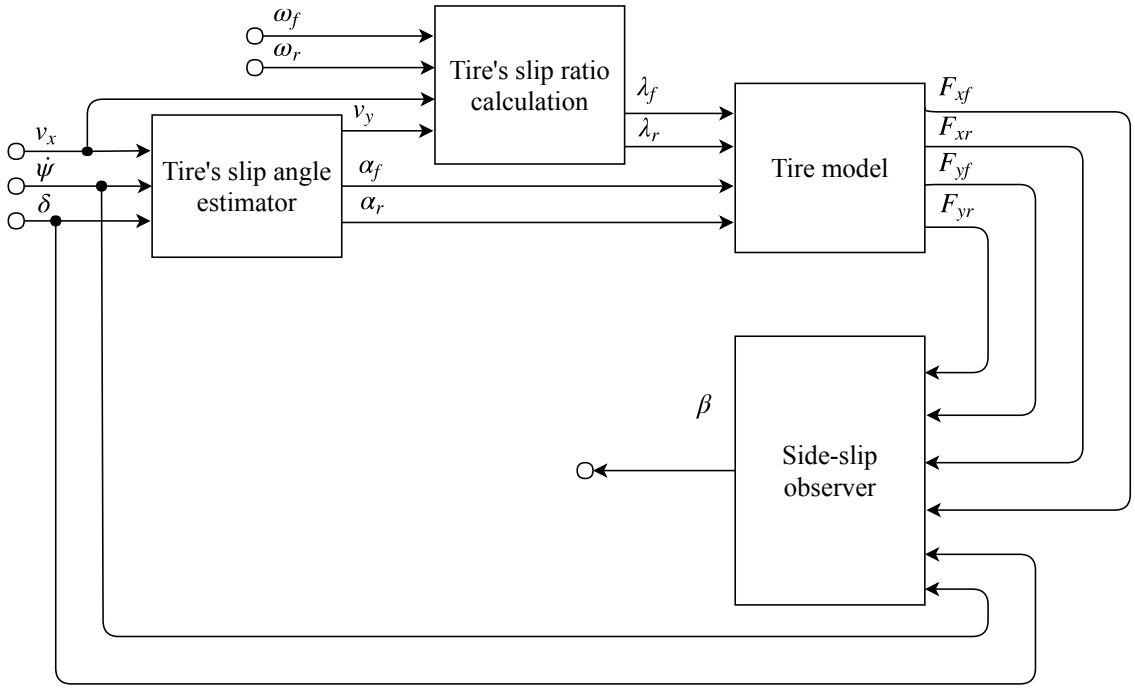

Figure 7.2: Diagram of vehicles's side-slip angle estimation

Tire's slip ratio can be calculated by the following formula taken from [1, chapter 7]:

$$\lambda = \frac{|v - \omega r|}{\max(v, \omega r)}, \quad \lambda \in [0, 1], \tag{7.4}$$

where $v \approx v_x + v_y$ is a velocity of the wheel center point, ω is an angular velocity of the wheel (typically is measured by rotation sensors), r is a wheel radius.

8. Force Feedback

The primary task of the whole thesis and the proposed control techniques above is to stabilize laterally unstable cars or improve their lateral characteristics. But that all is done by the cost of a real feeling of the tires and road of the traditional steering wheel because the steering wheel in these control approaches only introduces a reference but not the actual steering angle set on the front axle via the shaft. In vehicles, steered by regulators, are often used electronic (or electro-hydraulic) controllers instead of traditional hydraulic shafts, and these type systems are called steer-by-wire [9] car.

8.1 Overview of Steer-by-Wire Vehicles

The idea of using the steer-by-wire ground vehicles has the following profits for automotive companies and control engineers [10]:

- an open possibility of using new intelligent software and sensors feedback (as regulators, proposed in this work);
- modularity of the steering system so it can be adapted for different ground vehicles;
- lower manufacturing costs due to the reduction of used components (in case of a fully electronic steering column).

These type cars have the same problem as it was in avionics after the introduction of the fly-by-wire systems. How to create a drive-by-wire vehicle "feelable" like a traditional one? What forces and what feedback should the driver feel? Should he or she feel the actions caused by the regulator? Or should some next regulator be applied on the steering wheel to control the torque applied on the wheel by the force feedback? Or should it be done just by a combination of the measured and estimated values? While searching an answer to these questions we undoubtedly should focus on the avionics' force feedback solution.

8.2 The Implementation Used in This Thesis

There are many different approaches to generate the force feedback to the steering wheel starting from an option with augmented existing hydraulic shafts by pump controlled with the use of a load pressure feedback [10], finishing with an electric drive engine inside a steering wheel, which generates torque as a result of a combination of a feedback from the steering system model, a feedback from the vehicle dynamics and a filtered feedforward input signals taken from the stering wheel itself [9].

Simulator in this work implementes force feedback from the aligning torque (Figure 3.5) acting on the front tires in case of $\delta \neq 0$. This is a part of the implementation described by Paul Yih and J. Christian Gerdes in [9].

The paper referenced above has a good description of the aligning moment:"While a vehicle is turning, tire forces acting on the steering system tend to resist steering motion away from the straight-ahead position. These forces can be treated as a disturbance on the steering system and are directly attributable to tire self-aligning moment". But in this paper authors use the torque M_z as a function of the lateral force acting on tires F_y. This thesis' upgrade was to use the Pacejka Magic formula to calculate this torque directly from the tire slip angle. The used formula is discussed in chapter [**Used Vehicle Modelling Approaches**].

The used feedback is implemented as it is shown in Figure 8.1. The system's inputs are steering angle δ and force acting on the rear axle along the x axis in the vehicle coordinate system (Figure 3.1). They are used in the vehicle's model to calculate the front tire slip angle α_f and then the Pacejka Magic formula is applied to estimate the torque around the z axis in tire coordinate system (Figure 8.2). After that, the torque goes through a low-pass filter and then it is scaled, saturated and then applied on the electromotor inside the steering wheel.

The Figure 8.3 presents an example of the torque output together with yaw rate and the front tire's slip angle.

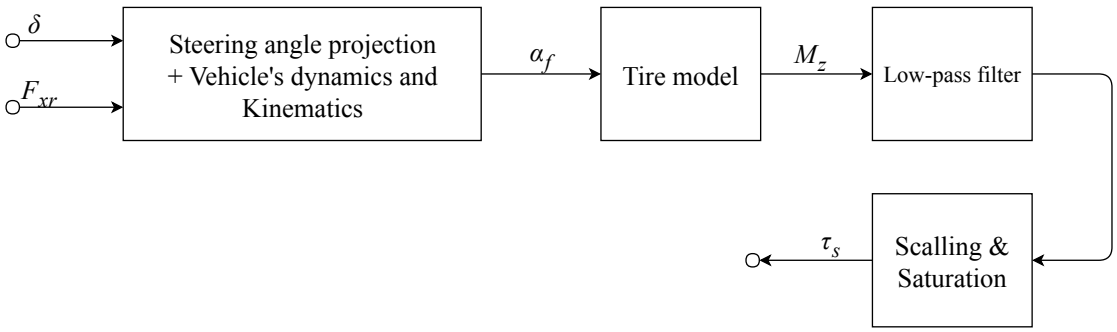

Figure 8.1: Implemented force feedback

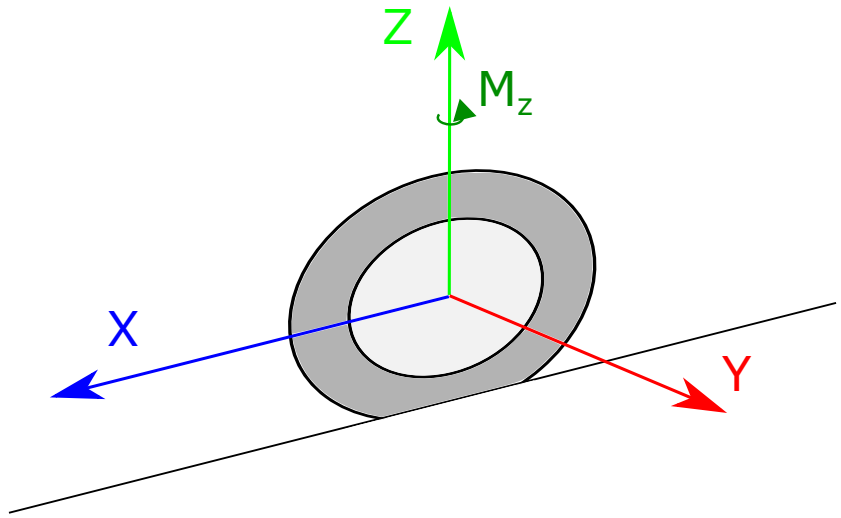

Figure 8.2: The tire coordinate system

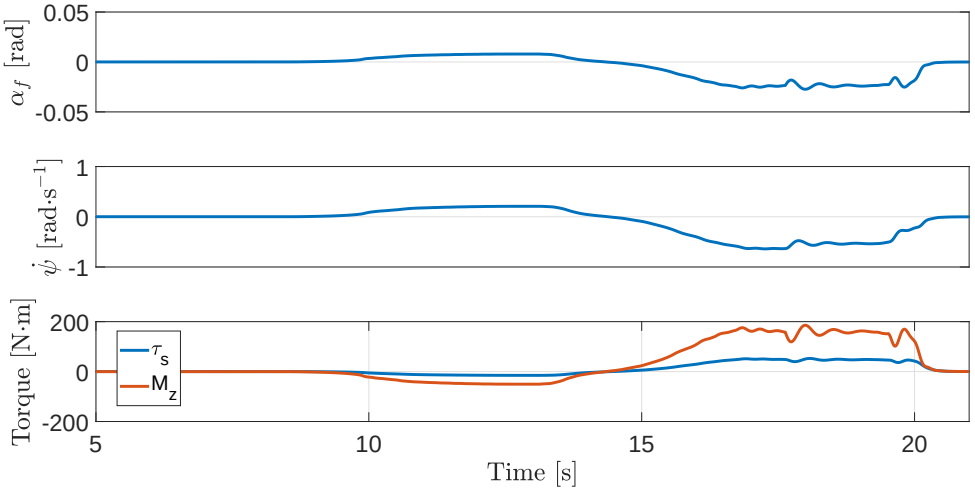

Figure 8.3: Example of the applied torque

9. Results

All of the goals, listed in chapter [**Objectives**], are done. Namely:

- Non-linear single-track model is created. Description of the used model is provided in chapter [**Used Vehicle Modelling Approaches**].
- The laterally unstable vehicle is defined in chapter [**Laterally Unstable Vehicle**].
- Implemented single-track model is connected with free simulator Panthera made by Cruden [**20**].
- Possible control architectures for laterally unstable ground vehicles are described in chapter [**Proposed Control Architectures**].
- Simulation tests are provided in chapter [**Simulation Tests**].
- Estimation algorithms for missing parameters are overviewed in chapter [**Slip Estimation Algoritms**].
- Additionally, a short overview of steer-by-wire vehicles is done in the chapter [**Force Feedback**].

10. Conclusion

This work completely answers a question named on the begging of this thesis: "What if we create a laterally unstable ground vehicle?" It has as its pros so its cons, namely, the main advantage is that unstable ground vehicle is agiler than stable (as it is in avionics), it is stabilizable, that is shown by provided simulation tests. Also, active stabilization can replace a rear wing used for passive vehicle stabilization at higher speeds.

But there are, as always, some cons. The laterally unstable ground vehicle should be equipped with the active steering system, the typical driver cannot stabilize this system by her or himself. Also, there is a necessity of using estimation algorithms for missing parameters for regulation and using force feedback to stay the car accustomed for the driver. But everything has a price. In avionics, this price was paid. What stops us to pay this price in automotive?

Despite the results achieved, this work opens a new field to the discussion. In the future work, there is a necessity to test proposed control techniques on a high-fidelity model (twin-track); research of other possible control techniques, which are not connected with yaw rate tracking; investigate a possibility of using state feedback regulation methods; discuss control techniques which guarantee the robustness of the stabilization.

All of the possibilities and goals listed above I am going to investigate and solve during my future Ph.D. education.

11. Bibliography

[1] Schramm, D., Hiller, M., & Bardini, R. (2014). Vehicle dynamics. *Modeling and Simulation. Berlin, Heidelberg*, 151.

[2] Ackermann, J. (1994). Robust decoupling, ideal steering dynamics and yaw stabilization of 4WS cars. *Automatica, 30*(11), 1761-1768.

[3] Guvenc, B. A., Guvenc, L., & Karaman, S. (2009). Robust yaw stability controller design and hardware-in-the-loop testing for a road vehicle. *IEEE Transactions on Vehicular Technology, 58*(2), 555-571.

[4] Wang, L., & Ackermann, J. (1998, June). Robustly stabilizing PID controllers for car steering systems. *In American Control Conference, 1998. Proceedings of the 1998* (Vol. 1, pp. 41-42). IEEE.

[5] Sienel, W. (1997, December). Estimation of the tire cornering stiffness and its application to active car steering. In *Decision and Control, 1997., Proceedings of the 36th IEEE Conference on* (Vol. 5, pp. 4744-4749). IEEE.

[6] Mondek M. (2018) *Active torque vectoring systems for electric drive vehicles* (Master thesis). Retrived from Czech Technical University Digital Library

[7] Haffner L. (2008) *Real-time tire models for lateral vehicle state estimation* (Doctoral dissertation). Retrived from Universitätsbibliothek der TU Wien

[8] Pacejka, H. (2005). *Tire and vehicle dynamics*. Elsevier.

[9] Yih, P., & Gerdes, J. C. (2005). M*odification of vehicle handling characteristics via steer-by-wire. IEEE Transactions on Control Systems Technology, 13*(6), 965-976.

[10] Haggag, S., Alstrom, D., Cetinkunt, S., & Egelja, A. (2005). Modeling, control, and validation of an electro-hydraulic steer-by-wire system for articulated vehicle applications. *IEEE/AsME Transactions on Mechatronics, 10*(6), 688-692.

[11] Ackermann, J. (2012). *Robust control: Systems with uncertain physical parameters.* Springer Science & Business Media.

[12] Takahashi, T. (2003). Modeling, analysis and control methods for improving vehicle dynamic behavior (overview). *R&D Review of Toyota CRDL, 38*(4), 1-9.

[13] SAE Surface Vehicle Recommended Practice, "Vehicle Dynamics Terminology," SAE Standard J670, Rev. Aug. 2008

[14] Vilela, D., & Barbosa, R. S. (2011). Analytical models correlation for vehicle dynamic handling properties. *Journal of the Brazilian Society of Mechanical Sciences and Engineering, 33*(4), 437-444.

[15] Baffet, G., Charara, A., & Lechner, D. (2009). Estimation of vehicle sideslip,

tire force and wheel cornering stiffness. *Control Engineering Practice, 17*(11), 1255-1264.

[16] Whitford, R. (1995, September). A fighter design chronology. In *Aircraft Engineering, Technology, and Operations Congress* (p. 3920).

[17] Sadettin Hamut, H., Salah El-Emam, R., Aydin, M., & Dincer, I. (2014). Effects of rear spoilers on ground vehicle aerodynamic drag. *International Journal of Numerical Methods for Heat & Fluid Flow, 24*(3), 627-642.

[18] Skogestad, S., & Postlethwaite, I. (2007). *Multivariable feedback control: analysis and design* (Vol. 2, pp. 359-368). New York: Wiley.

[19] Milliken, W. F., Milliken, D. L., Metz, L. D., & Kasprzak, E. M. (1997). Race Car Vehicle Dynamics Book and Problems, Answers and Solutions Set. *Warrendale, PA: Society of Automotive Engineers*, 1997. 990.

[20] Cruden official web-site: *http://www.cruden.com/panthera-software/*

List of Figures